Smoothed Particle Hydrodynamics Simulation of Water-Soil Mixture Flows

Chun Wang[1]; Yongqi Wang[2]; Chong Peng[3]; and Xiannan Meng[4]

Abstract: A two-phase smoothed particle hydrodynamics (SPH) mixture model to simulate water-soil interactions is presented. In this model, each phase of the mixture satisfies its own conservation equations of mass and momentum. The water is considered as a Newtonian fluid and the soil is modeled as an elastic-perfectly plastic material. Drucker-Prager criterion is employed to test the yielding of the soil and an associated flow rule is adopted to describe the soil behavior after yielding. Interactions between water and soil are modeled by the viscous drag force according to Darcy's law. With this mixture model, it is possible to investigate the temporal and spatial evolutions of the volume fractions of both phases. This study first examines the proposed SPH mixture model for two single-phase flows, i.e., water dam break and sand column collapse, respectively. The drag force model is also tested using the problem of flow in porous media. Then its application to the problem of soil excavation by high-velocity impinging water jets is illustrated. The flow pattern, profile of excavation hole, evolutions of pressure, volume fraction, and plastic shear strain during the impinging process are obtained and found to be qualitatively good compared with previous experimental observations and numerical simulations. Effects of hydraulic conductivity and initial volume fractions of water and soil on the excavation are revealed. Numerical simulation shows that the proposed method is robust and efficient, and can be applied to water-soil mixture flow problems in hydraulic engineering and geotechniques, especially to those cases where volume fractions play important roles in the mixture dynamics. **DOI: 10.1061/(ASCE)HY.1943-7900.0001163.** © *2016 American Society of Civil Engineers.*

Author keywords: Water-soil interactions; Two-phase mixture model; Water jetting; Numerical simulation; Smoothed particle hydrodynamics (SPH) method.

Introduction

Water-soil mixture flows occur widely in different fields. Typical examples include debris and mud flows (e.g., Bagnold 1954; Savage and Hutter 1989; Iverson and Denlinger 2001; Pitman and Le 2005; Pudasaini 2012); scour and erosion downstream the dam spillways or headcuts (e.g., Aderibigbe and Rajaratnam 1996; Mazurek et al. 2001); erosion of the channel bed or quay wall by the propellers of passing ships (Yeh et al. 2009); underwater soil excavation and trenching by means of high-velocity water jets (e.g., Perng and Capart 2008), to name a few. In these flows, water-soil interactions play an important role in the mixture dynamics.

During the last few decades, researchers have developed three kinds of water-soil interaction models: single phase models, quasi-single phase models, and multiphase mixture models. Single phase models, represented by viscoplastic model of Bagnold (1954) and Coulomb plastic model of Savage and Hutter (1989), treat the water-soil mixture as a single non-Newtonian fluid material. Because of the single phase hypothesis, such models are not able to describe the complex interactions between water and soil. Quasi-single phase models, as in Iverson and Denlinger (2001), consider the role of the pore water, but assume equal velocities for the constituents, which is inconsistent with the real situation.

In two-phase mixture models, as in Pitman and Le (2005) and Pudasaini (2012), each constituent satisfies its own mass and momentum conservation equations. The interactive coupling between the two constituents is modeled by the linear or quadratic viscous drag force. One of the advantages of the two-phase mixture models over the previous ones is that the spatial and temporal distributions of the volume fraction of each constituent can be investigated.

Although intensive studies have been conducted, water-soil interactions are still open questions due to the turbidity of the current and the complex behaviors of the soil. In water-soil mixture flows, soil undergoes large deformation that is difficult to treat using grid-based methods. Smoothed particle method (SPH), originally proposed by Gingold and Monaghan (1977) and Lucy (1977), is an appealing tool in dealing with large deformation problems, because of its Lagrangian and mesh free features. Bui et al. (2007) pioneered the numerical simulation of water-soil interactions using SPH method. They proposed a two-phase model, in which the water is regarded as a Newtonian fluid and the soil as an elastic-perfectly plastic material. Interactions between water and soil are modeled by the Darcy's law and pore water pressure. With the aid of this novel numerical method, some interesting phenomena of water-soil interactions have been revealed. Recently, Guo et al. (2013) revisited the same problem. However, in their model, water and soil are not allowed to merge with each other. Thus their model is in fact a two-phase immiscible flow model. There are some other works on numerical simulation of water-soil interaction

[1]Associate Professor, School of Naval Architecture, Ocean and Civil Engineering, Shanghai Jiao Tong Univ., 800 Dongchuan Rd., Shanghai 200240, China; Visiting Scientist and Chair of Fluid Dynamics, Dept. of Mechanical Engineering, Technische Universität Darmstadt, Otto-Berndt-Str. 2, 64287 Darmstadt, Germany (corresponding author).

[2]Professor, Chair of Fluid Dynamics, Dept. of Mechanical Engineering, Technische Universität Darmstadt, Otto-Berndt-Str. 2, 64287 Darmstadt, Germany.

[3]Postdoctoral, Institute of Geotechnical Engineering (IGT), Universitaet fuer Bodenkultur, Feistmantelstrasse 4, 1180 Vienna, Austria.

[4]Ph.D. Student, Chair of Fluid Dynamics, Dept. of Mechanical Engineering, Technische Universität Darmstadt, Otto-Berndt-Str. 2, 64287 Darmstadt, Germany.

Note. This manuscript was submitted on October 7, 2014; approved on February 17, 2016; published online on May 17, 2016. Discussion period open until October 17, 2016; separate discussions must be submitted for individual papers. This paper is part of the ***Journal of Hydraulic Engineering***, © ASCE, ISSN 0733-9429.

problems based on two-fluid SPH approaches. For example, Manenti et al. (2012) applied an SPH-based numerical model to analyze the coupled fluid-sediment dynamics induced by the rapid water discharge in an artificial reservoir. In their study, noncohesive sediments at the bottom are modeled in two different ways, i.e., at rest or eroded, according to the definition of a strength threshold. Both the liquid phase and the eroded granular particles are considered as weakly compressible fluids. Ulrich et al. (2013) studied the harbor bed erosion induced by the starting propeller of a large full-scale container vessel. The soil phase is treated as a viscous material with a variable viscosity. The models employed by both Manenti et al. (2012) and Ulrich et al. (2013) do not belong to the category of mixture models.

Because in saturated soil, each constituent (water and soil) occupies only part of the volume space in the macroscopic mixture modeling, the dynamics of the mixture will be influenced by the volume fraction of each phase. For instance, the drag force is related to the porosity, which is in fact the volume fraction of the water phase in saturated soil. None of the previously mentioned SPH simulations considered the effects of volume fractions on the dynamics of the mixture. In this paper, an SPH approximation of two-phase mixture model is formulated and applied to the problem of soil excavation by high-velocity water jets. In this model, there are two kinds of particles, i.e., water particles and soil particles, which are initially superimposed and then moving at different velocities according to their own mass and momentum equations. Volume fractions for water and soil particles are taken as field variables that should be determined together with other fundamental variables, such as density, stress, and velocity. With this mixture model, it is possible to investigate the temporal and spatial evolutions of the volume fractions of both phases. Effects of hydraulic conductivity and initial volume fractions of water and soil on the excavation are investigated, which helps to reveal the mechanisms of soil failure under the impingement of high velocity water jets.

In the following sections, mathematical formulation of the mixture theory is first presented, followed by the numerical implementation using SPH method. The proposed SPH two-phase mixture model is then validated by some typical problems such as water dam break, granular column collapse, and flow through porous media. Finally, this is applied to the problem of soil excavation by high-velocity water jets. Flow pattern, excavation profile, pressure, volume fraction, and plastic shear strain distribution at representative times during the impinging process are obtained and compared with previous experimental observations and numerical simulations to show the effectiveness of the proposed approach, with special focus on the capability to investigate effects of hydraulic conductivity and initial volume fractions on the mixture dynamics. Conclusions and remarks are made in the last section.

Mathematical Formulation

Water-Soil Mixture Model

Consider the saturated water-soil mixture flows. With the mixture theory (e.g., Drew 1983; Wang and Hutter 1999a, b), the mass conservation equations are given by

$$\partial_t(\tilde{\rho}_s\phi_s) + \nabla\cdot(\tilde{\rho}_s\phi_s\boldsymbol{v}_s) = 0 \tag{1}$$

$$\partial_t(\tilde{\rho}_f\phi_f) + \nabla\cdot(\tilde{\rho}_f\phi_f\boldsymbol{v}_f) = 0 \tag{2}$$

where subscripts s and f = soil and water, respectively; the density $\tilde{\rho}$ = true density of each constituent; ϕ = volume fraction; $\boldsymbol{v}$ = velocity with components v^α and v^β; ∂_t = partial derivative with respect to time t; and the nabla symbol ∇ = vector differential operator. Here, true density $\tilde{\rho}_f$ of water is the density of the interstitial water (also called pore water) in the mixture. True density $\tilde{\rho}_s$ of soil is the density of the particles that make up the soil, in contrast to the bulk density, which measures the average density of a large volume of the soil in a specific medium (usually air). True density of soil is thus defined as the mass per unit volume, not including the pore spaces in between the grains.

The volume fraction ϕ of a constituent at a given point and instant is defined as the percentage of volume occupied by this constituent within the local volume filled by water and soil at the same instant, and satisfies the following saturation relationship

$$\phi_f = 1 - \phi_s \tag{3}$$

Conservation equations for momentum are

$$\partial_t(\tilde{\rho}_s\phi_s\boldsymbol{v}_s) + \nabla\cdot(\tilde{\rho}_s\phi_s\boldsymbol{v}_s\boldsymbol{v}_s) = \nabla\cdot\hat{\boldsymbol{\sigma}}_s + \tilde{\rho}_s\phi_s\boldsymbol{g} + \boldsymbol{f}_s \tag{4}$$

$$\partial_t(\tilde{\rho}_f\phi_f\boldsymbol{v}_f) + \nabla\cdot(\tilde{\rho}_f\phi_f\boldsymbol{v}_f\boldsymbol{v}_f) = \nabla\cdot\hat{\boldsymbol{\sigma}}_f + \tilde{\rho}_f\phi_f\boldsymbol{g} - \boldsymbol{f}_s \tag{5}$$

where $\hat{\boldsymbol{\sigma}}_s$ and $\hat{\boldsymbol{\sigma}}_f$ = partial stresses of the soil and the water, respectively; $\boldsymbol{g}$ = gravitational acceleration; and $\boldsymbol{f}_s$ = interaction forces exerted on the soil phase by the water phase.

In momentum Eqs. (4) and (5), the form of the partial stress tensors $\hat{\boldsymbol{\sigma}}_s$ and $\hat{\boldsymbol{\sigma}}_f$ should be specified. For soil, assume that $\hat{\boldsymbol{\sigma}}_s = \phi_s\boldsymbol{\sigma}_s$, where $\boldsymbol{\sigma}_s$ is the stress tensor of the dry soil. For water, the relationship $\hat{\boldsymbol{\sigma}}_f = -p_f I + \phi_f\boldsymbol{\tau}_f$ is assumed, where p_f and $\boldsymbol{\tau}_f$ are the pore pressure and the shear stress of the water, respectively. The interaction force $\boldsymbol{f}_s$ is assumed to be composed of two parts: the buoyancy force $-\phi_s\nabla p_f$ and the viscous drag force $\boldsymbol{f}_d$. With these assumptions, the momentum equations can now be rewritten as

$$\partial_t(\tilde{\rho}_s\phi_s\boldsymbol{v}_s) + \nabla\cdot(\tilde{\rho}_s\phi_s\boldsymbol{v}_s\boldsymbol{v}_s) = \nabla\cdot(\phi_s\boldsymbol{\sigma}_s) + \tilde{\rho}_s\phi_s\boldsymbol{g} - \phi_s\nabla p_f + \boldsymbol{f}_d \tag{6}$$

$$\partial_t(\tilde{\rho}_f\phi_f\boldsymbol{v}_f) + \nabla\cdot(\tilde{\rho}_f\phi_f\boldsymbol{v}_f\boldsymbol{v}_f) = -\phi_f\nabla p_f + \nabla\cdot(\phi_f\boldsymbol{\tau}_f) + \tilde{\rho}_f\phi_f\boldsymbol{g} - \boldsymbol{f}_d \tag{7}$$

where the authors have made use of the saturation relationship in Eq. (4). Defining partial densities as $\rho_s = \tilde{\rho}_s\phi_s$, $\rho_f = \tilde{\rho}_f\phi_f$, mass conservation Eqs. (1) and (2) become

$$\frac{D^s\rho_s}{Dt} = -\rho_s\nabla\cdot\boldsymbol{v}_s \tag{8}$$

$$\frac{D^f\rho_f}{Dt} = -\rho_f\nabla\cdot\boldsymbol{v}_f \tag{9}$$

where $D^\iota(\cdot)/Dt$ = material time derivative with respect to $\boldsymbol{v}_\iota$ ($\iota = s, f$ denoting soil and fluid, respectively). Momentum Eqs. (6) and (7) become

$$\partial_t(\rho_s\boldsymbol{v}_s) + \nabla\cdot(\rho_s\boldsymbol{v}_s\boldsymbol{v}_s) = \nabla\cdot(\phi_s\boldsymbol{\sigma}_s) - \phi_s\nabla p_f + \rho_s\boldsymbol{g} + \boldsymbol{f}_d \tag{10}$$

$$\partial_t(\rho_f\boldsymbol{v}_f) + \nabla\cdot(\rho_f\boldsymbol{v}_f\boldsymbol{v}_f) = -\phi_f\nabla p_f + \nabla\cdot(\phi_f\boldsymbol{\tau}_f) + \rho_f\boldsymbol{g} - \boldsymbol{f}_d \tag{11}$$

Making use of the mass conservation Eqs. (8) and (9), the momentum equations can also be written as

$$\rho_s\frac{D^s\boldsymbol{v}_s}{Dt} = \nabla\cdot(\phi_s\boldsymbol{\sigma}_s) - \phi_s\nabla p_f + \boldsymbol{f}_d + \rho_s\boldsymbol{g} \tag{12}$$

$$\rho_f \frac{D^f \boldsymbol{v}_f}{Dt} = -\phi_f \nabla p_f + \nabla \cdot (\phi_f \boldsymbol{\tau}_f) - \boldsymbol{f}_d + \rho_f \boldsymbol{g} \tag{13}$$

Here, the governing Eqs. (8), (9), (12) and (13) are rewritten in Lagrangian form, facilitating numerical approximation using SPH method, which is based on Lagrangian formalism.

In this study, the true density $\tilde{\rho}_s$ of the soil is assumed to be constant. Thus the mass equation for soil becomes the governing equation for the volume fraction ϕ_s of soil. The volume fraction ϕ_f of water is calculated from the complementary condition in Eq. (4). In Eqs. (4), (8), (9), (12), and (13), there are six unknowns: ϕ_s, ϕ_f, ρ_f, $\boldsymbol{v}_s$, $\boldsymbol{v}_f$, and p_f. To close the system, it is necessary to specify the constitutive relations for the interaction forces and the stress tensors, which will be addressed in the next section.

Constitutive Model for Water

To simplify the representation, the authors make the convention that all variables appearing in this subsection are related to water. In the current study, the water phase is considered as a Newtonian fluid. The deviatoric stress tensor $\tau^{\alpha\beta}$ of the water is given by

$$\tau^{\alpha\beta} = \mu \varepsilon^{\alpha\beta} \tag{14}$$

where μ = dynamic viscosity of the water, and $\varepsilon^{\alpha\beta}$ is defined as

$$\varepsilon^{\alpha\beta} = \frac{\partial v^\beta}{\partial x^\alpha} + \frac{\partial v^\alpha}{\partial x^\beta} - \frac{2}{3}\left(\frac{\partial v^\gamma}{\partial x^\gamma}\right)\delta^{\alpha\beta} \tag{15}$$

where $\delta^{\alpha\beta}$ = Kronecker delta symbol; and γ = dummy index applicable to summation convention. For the waterjet impact problem investigated in this paper, the flow is dominated by the inertia, thus the laminar flow assumption is adopted for this study. For turbulence modeling in SPH, the readers may refer to Violeau and Issa (2007).

The relation between density and pore pressure, i.e., equation of state for water is taken as

$$p_f = B\left[\left(\frac{\tilde{\rho}}{\tilde{\rho}_0}\right)^\chi - 1\right] \tag{16}$$

where $\tilde{\rho}_0$ = reference true density of water; χ = constant normally set to seven; and B = problem dependent parameter that sets a limit for the maximum change of density. According to compressible flow theory, the sound speed of water is

$$c^2 = \left.\frac{\partial p_f}{\partial \tilde{\rho}}\right|_{\tilde{\rho}=\tilde{\rho}_0} = \frac{B\chi}{\tilde{\rho}_0} \tag{17}$$

The density variation $\delta\tilde{\rho} \equiv \tilde{\rho} - \tilde{\rho}_0$ is related to the Mach number M by Monaghan (1994)

$$\frac{\delta\tilde{\rho}}{\tilde{\rho}_0} \sim M^2 = \left(\frac{V}{c}\right)^2 \tag{18}$$

where V = typical velocity of the fluid. If B is chosen such that the density fluctuation of water is 1%, the result is $c^2 = 100V^2$, which when substituted into Eq. (17) gives

$$B = 100V^2\tilde{\rho}_0/\chi \tag{19}$$

The equation of state Eq. (16) can also be expressed in terms of partial densities as

$$p_f = B\left[\left(\frac{\tilde{\rho}\phi}{\tilde{\rho}_0\phi}\right)^\chi - 1\right] = B\left[\left(\frac{\rho}{\rho_0}\right)^\chi - 1\right] \tag{20}$$

where ρ_0 = reference partial density.

Constitutive Model for Soil

In this subsection, all variables are related to soil. Bui et al. (2008) and Bui and Fukagawa (2013) proposed an incremental plasticity model to describe the large deformation behavior of soil. This model is adopted here and depicted as follows.

The soil is considered as an elastic-perfectly plastic material. With the incremental plasticity theory, the constitutive relation of an elastic-perfectly plastic material is expressed as

$$\dot{\sigma}^{\alpha\beta} = 2\,G\dot{e}^{\alpha\beta} + K\dot{\epsilon}^{\gamma\gamma}\delta^{\alpha\beta} - \dot{\lambda}\left[\left(K - \frac{2}{3}G\right)\frac{\partial H}{\partial \sigma^{\gamma\gamma}}\delta^{\alpha\beta} + 2\,G\frac{\partial H}{\partial \sigma^{\alpha\beta}}\right] \tag{21}$$

where $\dot{\sigma}^{\alpha\beta}$ = stress rate tensor; and $\dot{\epsilon}^{\alpha\beta}$ = total strain rate tensor defined as

$$\dot{\epsilon}^{\alpha\beta} = \frac{1}{2}\left(\frac{\partial v^\alpha}{\partial x^\beta} + \frac{\partial v^\beta}{\partial x^\alpha}\right) \tag{22}$$

G = shear modulus; K = bulk modulus; G and K are related to the Young's modulus E and the Poisson's ratio ν through

$$K = \frac{E}{3(1-2\nu)}, \qquad G = \frac{E}{2(1+\nu)} \tag{23}$$

$\dot{e}^{\alpha\beta} = \dot{\epsilon}^{\alpha\beta} - 1/3(\dot{\epsilon}^{\gamma\gamma}\delta^{\alpha\beta})$ = deviatoric strain rate tensor; $\dot{\lambda}$ = rate of change of the plastic multiplier λ, which is dependent on the state of stress and load history; and H = plastic potential function needed in the flow rule. The flow rule defines the relationship between the next increment of the plastic strain and the present state of stress for a yield element subjected to further loading, i.e.

$$\dot{\epsilon}_p^{\alpha\beta} = \dot{\lambda}\frac{\partial H}{\partial \sigma^{\alpha\beta}} \tag{24}$$

In constitutive Eq. (21), $\dot{\lambda}$ is determined by the so-called consistency condition, which states that the stress state is always on the yield surface $F(\sigma^{\alpha\beta}) = 0$ during the plastic deformation. This condition can be written in the following form:

$$dF = \frac{\partial F}{\partial \sigma^{\alpha\beta}} d\sigma^{\alpha\beta} = \frac{\partial F}{\partial \sigma^{\alpha\beta}} \dot{\sigma}^{\alpha\beta} dt = 0 \tag{25}$$

Substituting Eq. (21) into Eq. (25), the general formulation for $\dot{\lambda}$ is obtained as

$$\dot{\lambda} = \frac{2G\dot{\epsilon}^{\alpha\beta}\frac{\partial F}{\partial \sigma^{\alpha\beta}} + (K - \frac{2G}{3})\dot{\epsilon}^{\gamma\gamma}\frac{\partial F}{\partial \sigma^{mm}}}{2G\frac{\partial F}{\partial \sigma^{mn}}\frac{\partial H}{\partial \sigma^{mn}} + (K - \frac{2G}{3})\frac{\partial F}{\partial \sigma^{mm}}\frac{\partial H}{\partial \sigma^{nn}}} \tag{26}$$

where summation convention is adopted for repeated indices. If the potential function and the yielding function coincide with each other (i.e., $F = H$), the flow rule is called the associated type, otherwise it is the nonassociated type. Two yield criteria, namely the Mohr-Coulomb (MC) and the Drucker-Prager (DP) yield criteria are commonly used in soil mechanics. According to Fourtakas et al. (2013), the DP yield criterion shows improvements over the MC criterion within the shear layer of the sediment. Thus, in this paper, the following Drucker-Prager yield criterion is chosen for soil

$$F(I_1, J_2) = \sqrt{J_2} + \alpha_\theta I_1 - k_c \tag{27}$$

where I_1 = first invariant of the total stress tensor; and J_2 = second invariant of the deviatoric stress tensor $\tau^{\alpha\beta}$. I_1 and J_2 are defined as

$$I_1 = \sigma^{xx} + \sigma^{yy} + \sigma^{zz}, \qquad J_2 = \frac{1}{2}\tau^{\alpha\beta}\tau^{\alpha\beta} \tag{28}$$

α_θ and k_c are constants that can be related to the cohesion and the friction angle θ of the Mohr-Coulomb failure criterion. In this paper, cohesion is considered as zero, thus $k_c = 0$. For plane strain problem, α_θ is determined by

$$\alpha_\theta = \frac{\tan\theta}{\sqrt{9 + 12\tan^2\theta}} \tag{29}$$

In this paper, the plastic potential function H is chosen to be equal to the yield function F, resulting the associated flow rule. Substituting F and H into Eq. (21), the constitutive equation becomes

$$\dot{\sigma}^{\alpha\beta} = 2\,G\dot{e}^{\alpha\beta} + K\dot{\epsilon}^{\gamma\gamma}\delta^{\alpha\beta} - \dot{\lambda}[3\alpha_\theta K\delta^{\alpha\beta} + G/\sqrt{J_2}\tau^{\alpha\beta}] \tag{30}$$

which is equivalent to

$$\dot{p}_s = -K\dot{\epsilon}^{\gamma\gamma} + 3\dot{\lambda}\alpha_\theta K \tag{31}$$

$$\dot{\tau}^{\alpha\beta} = 2G\dot{e}^{\alpha\beta} - \dot{\lambda}G/\sqrt{J_2}\tau^{\alpha\beta} \tag{32}$$

where $p_s = -\sigma^{\gamma\gamma}/3$ = isotropic part of tensor $\sigma^{\alpha\beta}$; while $\tau^{\alpha\beta}$ = the deviatoric part of $\sigma^{\alpha\beta}$. However, the previous relation for $\dot{\tau}^{\alpha\beta}$ does not satisfy the so-called material frame indifference (MFI) principle. In order to satisfy MFI, the Jaumann rate is adopted with the following constitutive equation

$$\dot{\tau}^{\alpha\beta} - \tau^{\alpha\gamma}\dot{\omega}^{\beta\gamma} - \tau^{\gamma\beta}\dot{\omega}^{\alpha\gamma} = 2G\dot{e}^{\alpha\beta} - \dot{\lambda}G/\sqrt{J_2}\tau^{\alpha\beta} \tag{33}$$

or equivalently

$$\dot{\tau}^{\alpha\beta} = \tau^{\alpha\gamma}\dot{\omega}^{\beta\gamma} + \tau^{\gamma\beta}\dot{\omega}^{\alpha\gamma} + 2G\dot{e}^{\alpha\beta} - \dot{\lambda}G/\sqrt{J_2}\tau^{\alpha\beta} \tag{34}$$

where the rotational rate tensor $\dot{\omega}^{\alpha\beta}$ is defined as

$$\dot{\omega}^{\alpha\beta} = \frac{1}{2}\left(\frac{\partial v^\alpha}{\partial x^\beta} - \frac{\partial v^\beta}{\partial x^\alpha}\right) \tag{35}$$

With the associated flow rule, the rate of change of plastic multiplier $\dot{\lambda}$ is calculated by

$$\dot{\lambda} = \frac{3\alpha_\theta K\dot{\epsilon}^{\gamma\gamma} + (G/\sqrt{J_2})\tau^{\alpha\beta}\dot{\epsilon}^{\alpha\beta}}{9\alpha_\theta^2 K + G} \tag{36}$$

Drag Force Model

In this paper, the viscous drag force $\boldsymbol{f}_d$ is assumed to be linear with respect to the velocity difference between the two phases, i.e., $\boldsymbol{f}_d = C_d(\boldsymbol{v}_f - \boldsymbol{v}_s)$, where the coefficient C_d can be derived from Darcy's law

$$C_d = \phi_f\gamma_w/k \tag{37}$$

where k = hydraulic conductivity with the dimensions of velocity [LT^{-1}]; $\gamma_w = \rho_f g$ = specific weight expressed with the partial density ρ_f of water; and k = constant depending not only on the type of soil but also on the type of fluid (dynamic viscosity μ) percolating through it. Values of hydraulic conductivity can be obtained from empirical formulas, laboratory experiments, or field tests (Nield and Bejan 2006).

From the previous governing equations and drag force calculation, it is shown that volume fractions affect the dynamics of the soil-water coupled flows. This is the core modeling concept for interpenetrating disperse flow, i.e., mixture flow. With the mixture theory, it is possible to investigate the effects of the volume fractions on the mixture dynamics.

SPH Implementation

Basic Idea of SPH Method

A brief introduction to SPH method is presented in this section for completeness. Detail can be found in Liu and Liu (2003), Monaghan (2005), and Violeau (2012). The foundation of SPH method is interpolation theory. The interpolation process is based on the following integral representation of a field function $f(\boldsymbol{x})$:

$$\langle f(\boldsymbol{x})\rangle = \int_\Omega f(\boldsymbol{x}')W(\boldsymbol{x} - \boldsymbol{x}', h)d\Omega \tag{38}$$

where W = kernel or smoothing function; and h = smoothing length defining the influence domain Ω of W. The smoothing function satisfies the normalization condition

$$\int_\Omega W(\boldsymbol{x} - \boldsymbol{x}', h)d\Omega = 1 \tag{39}$$

the delta condition

$$\lim_{h\to 0} W(\boldsymbol{x} - \boldsymbol{x}', h) = \delta(\boldsymbol{x} - \boldsymbol{x}') \tag{40}$$

and the compact condition

$$W(\boldsymbol{x} - \boldsymbol{x}', h) = 0, \qquad \text{for } |\boldsymbol{x} - \boldsymbol{x}'| > \kappa h \tag{41}$$

where κ is a constant. In Eq. (40), the Dirac delta function $\delta(\boldsymbol{x})$ in an n-dimensional Euclidean space $\boldsymbol{R}^n$ is defined by

$$\delta(\boldsymbol{x}) = \begin{cases} \infty, & \boldsymbol{x} = \boldsymbol{0}, \\ 0, & \boldsymbol{x} \neq \boldsymbol{0}. \end{cases}, \qquad \text{with } \int_{\boldsymbol{R}^n} \delta(\boldsymbol{x})d\boldsymbol{x} = 1 \tag{42}$$

A number of smoothing functions have been proposed in the literature. Among others, the Wendland kernel function (Wendland 1995) has been proven to be accurate and efficient. This smoothing function is employed in the current study and can be expressed as

$$W(R, h) = \alpha_d \times \begin{cases} (1 - R/2)^4(2R + 1), & 0 \le R \le 2, \\ 0, & R \ge 2 \end{cases} \tag{43}$$

where $R = |\boldsymbol{x} - \boldsymbol{x}'|/h$; and $\alpha_d = 7/(4\pi h^2)$ for two dimensional space.

In SPH method, the computational domain is discretized into a finite number of particles (Fig. 1). These particles carry material properties such as mass, density, velocity, and stress, and move with the material velocity according to the governing equations. The continuous integral representation of the field variable $f(\boldsymbol{x})$ in Eq. (38) can then be approximated by summation over the neighboring particles in the support domain, as

$$\langle f(\boldsymbol{x}_i)\rangle \approx \sum_j \frac{m_j}{\rho_j} f(\boldsymbol{x}_j)W_{ij} \tag{44}$$

where $W_{ij} = W(|\boldsymbol{x}_i - \boldsymbol{x}_j|, h)$; m_j and ρ_j = mass and density of particle j at position $\boldsymbol{x}_j$, respectively; the fraction m_j/ρ_j gives the volume ΔV_j of particle j, $j = 1,2,\ldots,N$; and N = number of particles in the support domain of particle i.

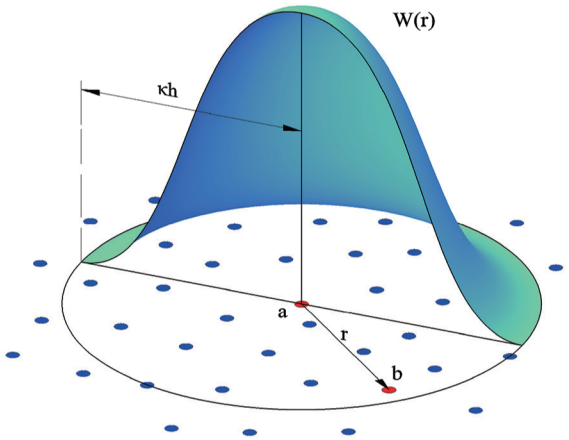

Fig. 1. Particle approximation in SPH method

The continuous integral approximation for the spatial derivative of the function $f(\boldsymbol{x})$ is

$$\langle \nabla_{\boldsymbol{x}} \cdot f(\boldsymbol{x}) \rangle = -\int_{\Omega} f(\boldsymbol{x}') \cdot \nabla_{\boldsymbol{x}'} W(\boldsymbol{x}-\boldsymbol{x}', h) d\Omega = \int_{\Omega} f(\boldsymbol{x}') \cdot \nabla_{\boldsymbol{x}} W(\boldsymbol{x}-\boldsymbol{x}', h) d\Omega \quad (45)$$

Here the symbol $\nabla \cdot$ can be gradient or divergence, according to whether the function $f(\boldsymbol{x})$ is a scalar function or a vector function, respectively. It is shown that the differential operation on function $f(\boldsymbol{x})$ has been transformed to the differential operation on the smoothing function W. In the derivation of Eq. (45), the authors have made use of the compact support condition in Eq. (41) and assumed that the integration point $\boldsymbol{x}$ is remote from the domain boundaries. In terms of discretized domain, the particle approximation for the spatial derivative of the function $f(\boldsymbol{x}_i)$ is

$$\langle \nabla \cdot f(\boldsymbol{x}_i) \rangle = \sum_j \frac{m_j}{\rho_j} f(\boldsymbol{x}_j) \cdot \nabla_i W_{ij} \quad (46)$$

where

$$\nabla_i W_{ij} = \frac{\boldsymbol{x}_i - \boldsymbol{x}_j}{r_{ij}} \frac{\partial W_{ij}}{\partial r_{ij}} = \frac{\boldsymbol{r}_{ij}}{r_{ij}} \frac{\partial W_{ij}}{\partial r_{ij}} \quad (47)$$

There are some alternative SPH formulations for the derivatives of function $f(\boldsymbol{x})$. For instance, making use of the following identities

$$\rho \nabla \cdot f(\boldsymbol{x}) = \nabla \cdot [\rho f(\boldsymbol{x}) - f(\boldsymbol{x}) \cdot \nabla \rho \quad (48)$$

$$\rho^{-1} \nabla \cdot f(\boldsymbol{x}) = \nabla \cdot \left[\frac{f(\boldsymbol{x})}{\rho}\right] + \frac{f(\boldsymbol{x})}{\rho^2} \cdot \nabla \rho \quad (49)$$

the derivatives of $f(\boldsymbol{x})$ can also be written as

$$\langle \nabla \cdot f(\boldsymbol{x}_i) \rangle = \frac{1}{\rho_i} \sum_j m_j [f(\boldsymbol{x}_j) - f(\boldsymbol{x}_i)] \cdot \nabla_i W_{ij} \quad (50)$$

$$\langle \nabla \cdot f(\boldsymbol{x}_i) \rangle = \rho_i \sum_j m_j \left[\frac{f(\boldsymbol{x}_i)}{\rho_i^2} + \frac{f(\boldsymbol{x}_j)}{\rho_j^2}\right] \cdot \nabla_i W_{ij} \quad (51)$$

Detailed derivation of SPH method are given in Liu and Liu (2003).

SPH Model for Water-Soil Mixture

Monaghan and Kocharyan (1995) and Monaghan (1997) made the first attempt to deal with two-phase flows using SPH. Although their idea is originally proposed for dusty gas problem, it can also be extended to water-soil interaction problems. In this section, an SPH approximation of two-phase mixture model for water-soil interaction problems is formulated. In this model, there are two kinds of particles, i.e., water particles and soil particles, which are initially superimposed and then moving at different velocities according to their own mass and momentum equations. For simplicity, the quantities for the water particles are identified by subscripts a and b, and for the soil particles by i and j. Applying the SPH particle approximations in Eqs. (50) and (51) to the gradients, the continuity equations in the SPH formulation will be

$$\frac{D^f \rho_a}{Dt} = \sum_b m_b (v_a^\alpha - v_b^\alpha) \frac{\partial W_{ab}}{\partial x_a^\alpha} + \delta_f h_a c_f \sum_b \psi_{ab}^\alpha \frac{m_b}{\rho_b} \frac{\partial W_{ab}}{\partial x_a^\alpha} \quad (52)$$

$$\frac{D^s \rho_i}{Dt} = \sum_j m_j (v_i^\alpha - v_j^\alpha) \frac{\partial W_{ij}}{\partial x_i^\alpha} + \delta_s h_i c_s \sum_b \psi_{ij}^\alpha \frac{m_j}{\rho_j} \frac{\partial W_{ij}}{\partial x_i^\alpha} \quad (53)$$

where h_a, h_i = smoothing lengths of particles a and i, respectively; c_f and c_s = reference sound speeds of water and soil, respectively; δ_f and δ_s = constants normally set to 0.1; and ψ_{ij} is

$$\psi_{ij} = 2(\rho_i - \rho_j) \frac{\boldsymbol{r}_{ij}}{|r_{ij}|^2} \quad (54)$$

where $\boldsymbol{r}_{ij} = \boldsymbol{x}_i - \boldsymbol{x}_j$. $\psi_{\alpha\beta}$ can be deduced analogously. The last terms in Eqs. (52) and (53) are added to avoid the density fluctuation, according to the so-called δ-SPH method, recently developed by Antuono et al. (2010) and Marrone et al. (2011a, b). In this study, the smoothing length is assumed as constant, thus the result is $h_a = h_i = h$ for all particles.

The SPH approximation for the momentum equation of soil is

$$\frac{D^s v_i^\alpha}{Dt} = -\sum_j m_j \left(\frac{p_i \phi_i}{\rho_i^2} + \frac{p_j \phi_j}{\rho_j^2} + \Pi_{ij}\right) \frac{\partial W_{ij}}{\partial x_i^\alpha} + \sum_j m_j \left(\frac{\tau_i^{\alpha\beta} \phi_i}{\rho_i^2} + \frac{\tau_j^{\alpha\beta} \phi_j}{\rho_j^2}\right) \frac{\partial W_{ij}}{\partial x_i^\beta} - \phi_i \sum_a m_a \frac{p_a}{\rho_i \rho_a} \frac{\partial W_{ia}}{\partial x_i^\alpha} + \sum_a^N m_a \frac{f_{ia}^\alpha}{\rho_i \rho_a} W_{ia} + g_i^\alpha \quad (55)$$

where p_a = pore water pressure of water particles calculated by Eq. (20); and p_i = pressure of soil particles calculated according to Eq. (31). In order to construct an SPH approximation for momentum equation of water, which conserve linear and angular momentum, it is necessary to write the pressure term in Eq. (13) in the form (Monaghan and Kocharyan 1995; Monaghan 1997)

$$-\phi_f \nabla p_f = -\nabla(p_f \phi_f) - p_f \nabla \phi_s \quad (56)$$

where use has been made of $\nabla \phi_f = -\nabla \phi_s$. Thus momentum Eq. (13) can be recast to

$$\rho_f \frac{D^f \boldsymbol{v}_f}{Dt} = -\nabla(p_f \phi_f) - p_f \nabla \phi_s + \nabla \cdot (\phi_f \boldsymbol{\tau}_f) - \boldsymbol{f}_d + \rho_f \boldsymbol{g} \quad (57)$$

The SPH approximation of the previous equation is

$$\frac{D^f v_a^\alpha}{Dt} = -\sum_b m_b \left(\frac{p_a\phi_a}{\rho_a^2} + \frac{p_b\phi_b}{\rho_b^2} + \Pi_{ab}\right)\frac{\partial W_{ab}}{\partial x_a^\alpha} + \sum_b m_b \left(\frac{\tau_a^{\alpha\beta}\phi_a}{\rho_a^2} + \frac{\tau_b^{\alpha\beta}\phi_b}{\rho_b^2}\right)\frac{\partial W_{ab}}{\partial x_a^\beta} - \sum_i m_i \frac{p_a\phi_i}{\rho_a\rho_i}\frac{\partial W_{ia}}{\partial x_a^\alpha} - \sum_i m_i \frac{f_{ia}^\alpha}{\rho_i\rho_a} W_{ia} + g_a^\alpha \tag{58}$$

In Eqs. (55) and (58), Π_{ij} and Π_{ab} are artificial viscosity terms added to prevent unphysical penetration of particles. Π_{ij} is defined as (Monaghan 1994)

$$\Pi_{ij} = \begin{cases} \dfrac{-\eta_1 \bar{c}_{ij}\phi_{ij} + \eta_2\phi_{ij}^2}{\bar{\rho}_{ij}}, & \boldsymbol{v}_{ij}\cdot\boldsymbol{r}_{ij} < 0, \\ 0, & \boldsymbol{v}_{ij}\cdot\boldsymbol{r}_{ij} \geq 0 \end{cases} \tag{59}$$

in which

$$\phi_{ij} = \frac{\bar{h}_{ij}\boldsymbol{v}_{ij}\cdot\boldsymbol{r}_{ij}}{|r_{ij}|^2 + \epsilon\bar{h}_{ij}^2}, \qquad \bar{c}_{ij} = \frac{1}{2}(c_i + c_j) \tag{60}$$

$$\bar{h}_{ij} = \frac{1}{2}(h_i + h_j), \qquad \bar{\rho}_{ij} = \frac{1}{2}(\rho_i + \rho_j) \tag{61}$$

where ϵ = small constant usually set to 0.01. Π_{ab} can be defined analogously by replacing i, j with a, b. Note that the internal forces (including pressure forces, shear stresses, and artificial viscous forces) occur in symmetric form ensuring Newton's third law, which is the conservation of the total momentum of an isolated system. For water, the two constants η_1, η_2 take values of 0.01 and 1, respectively, while for soil they are set to 0.1 and 1, respectively. Artificial viscosity should be included with care, because large artificial viscosity will lead to unphysical results. For example, the liquid flows much more slowly if large artificial viscosity is added. In some validation cases presented in this paper, such as the cases of water dam break and sand column collapse, the computation is still stable even without artificial viscosity. Discussions about artificial viscosity can be found, for example, in Colagrossi and Landrini (2003).

The deviatoric stress $\tau_a^{\alpha\beta}$ of water particles is calculated according to Eq. (14), where the SPH approximation of the deviatoric strain rate tensor $\varepsilon_a^{\alpha\beta}$ for water particle a is

$$\varepsilon_a^{\alpha\beta} = \sum_b \frac{m_b}{\rho_b} v_{ba}^\beta \frac{\partial W_{ab}}{\partial x_a^\alpha} + \sum_b \frac{m_b}{\rho_b} v_{ba}^\alpha \frac{\partial W_{ab}}{\partial x_a^\beta} - \left(\frac{2}{3}\sum_b \frac{m_b}{\rho_b}\boldsymbol{v}_{ba}\cdot\nabla_a W_{ab}\right)\delta^{\alpha\beta} \tag{62}$$

where $\boldsymbol{v}_{ba} = \boldsymbol{v}_b - \boldsymbol{v}_a$.

The discretized forms of the constitutive relations in Eqs. (31) and (34) for soil particle i are

$$\dot{p}_i = -K\dot{\epsilon}_i^{\gamma\gamma} + 3\dot{\lambda}_i\alpha_\theta K \tag{63}$$

$$\dot{\tau}_i^{\alpha\beta} = \tau_i^{\alpha\gamma}\dot{\omega}_i^{\beta\gamma} + \tau_i^{\gamma\beta}\dot{\omega}_i^{\alpha\gamma} + 2G\dot{e}_i^{\alpha\beta} - \dot{\lambda}_i G/\sqrt{J_{2i}}\tau_i^{\alpha\beta} \tag{64}$$

respectively, where the strain rate tensor $\dot{\epsilon}_i^{\alpha\beta}$ and the rotation rate tensor $\dot{\omega}_i^{\alpha\beta}$ are approximated as

$$\dot{\epsilon}_i^{\alpha\beta} = \frac{1}{2}\sum_j \left(\frac{m_j}{\rho_j} v_{ji}^\beta \frac{\partial W_{ij}}{\partial x_i^\alpha} + \frac{m_j}{\rho_j} v_{ji}^\alpha \frac{\partial W_{ij}}{\partial x_i^\beta}\right) \tag{65}$$

$$\dot{\omega}_i^{\alpha\beta} = \frac{1}{2}\sum_j \left(\frac{m_j}{\rho_j} v_{ji}^\beta \frac{\partial W_{ij}}{\partial x_i^\alpha} - \frac{m_j}{\rho_j} v_{ji}^\alpha \frac{\partial W_{ij}}{\partial x_i^\beta}\right) \tag{66}$$

according to Eqs. (22) and (35), respectively.

Calculation of the volume fraction for soil particle i is straightforward: once ρ_i has been found, ϕ_i can be calculated from $\rho_i = \tilde{\rho}_s\phi_i$ because $\tilde{\rho}_s$ is constant. Volume fraction ϕ_a for a water particle a is calculated from the relation from Eq. (4) in the form

$$\phi_a = 1 - \sum_j \frac{m_j}{\rho_j}\phi_j W_{aj} \tag{67}$$

where the summation gives the soil volume fraction ϕ_f at the position of water particle a. Eq. (67) can be written as

$$\phi_a = 1 - \frac{1}{\tilde{\rho}_s}\sum_j m_j W_{aj} \tag{68}$$

so that, recalling $\tilde{\rho}_s$ is constant

$$\frac{D^f\phi_a}{Dt} = -\frac{1}{\tilde{\rho}_s}\sum_j m_j \boldsymbol{v}_{aj}\cdot\frac{\partial W_{aj}}{\partial \boldsymbol{x}_a} \tag{69}$$

Eq. (69) leads to a more stable calculation, thus in the current study, the authors use Eq. (69) rather than Eq. (68).

Plasticity Treatment

The constitutive models of soil, e.g., Eqs. (63) and (64), contain terms related with the plastic multiplier. If the stress state is inside or on the yielding surface there is no need to compute these terms because the material is still in the elastic regime. This term only needs to be computed when the stress state is outside of the yield surface. In computational plasticity (e.g., de Souza Neto et al. 2011), this is done by the so-called return mapping algorithm, which normally consists of two steps to proceed: (1) the elastic trial step, and (2) the plastic corrector step. In the current study, an explicit treatment of the return mapping algorithm is employed. To do so, calculate the yield function $F(I_1, J_2)$ and the rate of change of the plastic multiplier $\dot{\lambda}$ using the stress tensor at the current time step t_n. When $F(I_1, J_2) \geq 0$ and $\dot{\lambda} > 0$, the particle is assumed to undergo plastic loading, then the plastic part of the stress rate tensor is added. Otherwise, the plastic part is set to zero.

Explicit integration of the stress rate tensor may lead to a stress state that lies outside the yield surface when yielding occurs. An explicit correction method proposed by Chen and Mizuno (1990), and recently applied by Bui et al. (2008), is employed to scale the stresses exceeding the yield strength back to the yield surface. This method involves two consequent steps, i.e., the tension cracking treatment and the stress-scaling back procedure. Tension cracking corresponds to the case where the stress state of soil moves beyond the apex of the yield surface. In this case, the particle is in tension, which is not allowed for noncohesive soil. To remove this tension cracking, the stress state is directly shifted to that at the apex. However, it should be pointed out that this treatment is valid only for noncohesive soil. For cohesive soil, an artificial stress method proposed by Monaghan (2000) and Gray et al. (2001) should be applied.

If the stress moves to above the Drucker-Pager surface (a line in 2D space), the stress at the end of step has to be reduced to return

the stress state back to the yield surface. This is called the stress-scaling back procedure. In this procedure, the deviatoric shear stress components are reduced in proportion to a scaling factor, whereas the hydrostatic stress component I_1 remains unchanged. The scaling factor is determined such that the new stress state is on the yield surface. For more details, refer to Bui et al. (2008).

Boundary Treatment and Time Stepping

In all the simulations, rigid wall boundaries are treated by the dynamic particle method (e.g., Crespo et al. 2007; Gomez-Gesteira et al. 2012). With this method, the boundary is replaced by several layers of virtual particles carrying mass, density, velocity, volume fraction, and stress as the real particles in the domain. Virtual particles are also involved in the calculation. Field variables of virtual particles, except velocity and position, evolve with time. The virtual particles produce repulsive force against real particles, thus preventing these particles from nonphysically penetrating the boundary. Recently, a more elegant method, namely the unified semianalytical wall boundary treatment method (USAM), was proposed by Ferrand et al. (2013). By solving a dynamic equation for the renormalizing factor, they significantly improved traditional wall treatment in SPH, for pressure forces, wall friction, and turbulence conditions. In fact, the idea of semianalytical treatment of solid boundary can also be found in an earlier paper by Monaco et al. (2011), where the solid boundary intersected with the support domain of a particle is replaced by a virtual fluid region with a suitable distribution of velocity, density, and pressure. With this method, the domain integrals over the virtual fluid region can be computed analytically. Because the flows in the current study are dominated by inertia rather than wall effects, the authors adopt the dynamic particle method to treat the boundaries for simplicity. Application of the more elegant boundary treatment method USAM will be a future topic.

When a water particle moves close to the free surface, the kernel function will be truncated, and the SPH approximation is no longer accurate, leading to the so-called problem of boundary deficiency. In this paper, the water density is calculated by the continuity Eq. (52). To overcome the problem of boundary deficiency, the authors reinitialize the density field every some time steps, according to the following summation density approach (see also Liu and Liu 2003; Gomez-Gesteira et al. 2012 for reference)

$$\rho_a = \frac{\sum_b m_b W_{ab}}{\sum_b (\frac{m_b}{\rho_b}) W_{ab}} \tag{70}$$

In this paper, time stepping is performed using second order Leap-Frog algorithm. In this method, field variables X, including velocity ($\boldsymbol{v}$), density (ρ), soil pressure (p_s), stress tensor (σ), and water volume fraction ( ) are offset from particle position ($\boldsymbol{x}$) by half a time step as shown in the following equations:

$$X_{n+1/2} = X_{n-1/2} + \Delta t \cdot \left(\frac{DX}{Dt}\right)_n \tag{71}$$

$$\boldsymbol{x}_{n+1} = \boldsymbol{x}_n + \Delta t \cdot \boldsymbol{v}_{n+1/2} \tag{72}$$

where Δt = time step size; n = current time step t_n; and $n+1$ = advanced time step ($t_n + \Delta t$). While the soil pressure p_s in Eq. (63) is updated using Eq. (71), the pore water pressure p_f should be updated according to the equation of state of Eq. (20).

Note that Leap-Frog only computes velocities and stresses at half steps. However, to compute the acceleration $(DX/Dt)_n$ at time t_n, it is necessary to obtain the velocity $\boldsymbol{v}_n$ and stress $\tau_n^{\alpha\beta}$ at integer time t_n, as seen in Eqs. (55), (58), and (64). Here, when computing the half-step velocity $\boldsymbol{v}_{n-1/2}$ and stress $\tau_{n-1/2}^{\alpha\beta}$, it is necessary to simultaneously compute an approximate integer step velocity $\boldsymbol{v}_n$ and stress $\tau_n^{\alpha\beta}$ by taking another half step using the acceleration $(DX/Dt)_{n-1}$. This has been tested with satisfactory results and is used in the simulations.

Because the stress states for soil are computed at each half time step and integer time step, the tension cracking treatment and the stress-scaling back procedure should be performed at each half and integer time step, ensuring that the stress states are inside or on the yield surface.

The time step size is controlled by the so-called Courant-Fredrich-Levy (CFL) condition

$$\Delta t \le C_{\text{cour}} \min(h/c_s, h/c_f) \tag{73}$$

where C_{cour} = Courant coefficient; h = smoothing length of particles; and c_f and c_s = sound speed of water and soil, respectively. The Courant coefficient is chosen to be $C_{\text{cour}} = 0.3$. Theoretically speaking, time step size is also affected by the physical viscosity, as shown for example in Monaco et al. (2011). However, in the current study, the viscosity stability condition is automatically satisfied by Eq. (73) due to the fact that the flows investigated in this paper are in convective dominant regime.

Initialization of the physical variables (e.g., pressure, density, and stresses) is worth mentioning. In the present SPH mixture model, the water is considered as weakly compressible, thus the initial density of the water should be adjusted according to the hydrostatic pressure of an incompressible fluid and the of state Eq. (20) of water, that is, the initial density of water particles is calculated by

$$\rho|_{t=0} = \rho_0 (p_f/B + 1)^{1/\chi} \tag{74}$$

where $p_f = \tilde{\rho}_0 g z$ = hydrostatic pressure of an incompressible fluid; and z = pressure head.

The static stress state in soil is very complex considering the plastic behavior of the material. In the current study, the initial normal stress in static soil is calculated by

$$\sigma_{xx} = \sigma_{yy} = K_0 \sigma_{zz} \tag{75}$$

where σ_{zz} = vertical stress; σ_{xx} and σ_{yy} = lateral (horizontal) stress; and K_0 = so-called coefficient of lateral earth pressure, which is related to the Poisson's ratio by

$$K_0 = \frac{\nu}{1-\nu} \tag{76}$$

Shear stress σ_{xy} is always set to zero for static soil.

To get the mass of each particle, the computational domain is discretized into cells with equal size. The mass m_i of a soil particle i is calculated by

$$m_i = \tilde{\rho}_i \delta V_i \phi_i = \rho_i \delta V_i \tag{77}$$

where $\tilde{\rho}_i$ and ρ_i = true density and partial density, respectively; and δV_i = initial volume of cell i. The mass of a soil particle a can be calculated analogously. The mass of each particle is assigned at the beginning of the computation and remains invariant during the time stepping. In the computation, the smoothing length is set to be constant, being equal to the initial particle spacing.

Table 1. Parameters Used in the Computation for the Water Dam Break Problem

Parameter	Symbol	Value
Reference density of water	$\tilde{\rho}_{f0}$	1,000 kg/m^3
Dynamic viscosity of water	μ	1.0×10^{-3} Pa · s
Virtual sound speed in water	c_f	25 m/s
Time step size	Δt	1.0×10^{-5} s

Simulations and Results Analysis

In this section, the SPH models are validated for single-phase flows using two standard examples, i.e., problems of water dam break and soil column collapse. The model for drag force between phases is validated using the flow in a porous medium. Then the proposed SPH mixture model is applied to the problem of soil excavation by high-velocity water jets.

Water Dam Break

First, the water dam break problem is employed to validate the SPH model for the water phase. In this example, the collapse of a 2D water column in a tank is simulated. This problem was investigated by Koshizuka and Oka (1996) both experimentally and numerically in a 2D domain. It became a classic example to test the validation of the Lagrangian formulation in fluid flow (Colagrossi and Landrini 2003; Idelsohn et al. 2004). The initial water column is 0.1 m wide and 0.2 m high, and the tank is 0.4 m wide and 0.2 m high. At $t = 0$, the water column collapses and particles move to the right. In the simulation, the water column is represented by a total of 12,800 water particles. The initial particle distance is 0.00125 m. Parameters used in the computation for this case is listed in Table 1. The virtual sound speed in water is taken as $c_f =$ 25 m/s, which corresponds to a typical water velocity of 2.5 m/s. Hereafter, for all the computations presented in this paper, the smoothing length h is taken as the same as the initial inter-particle distance.

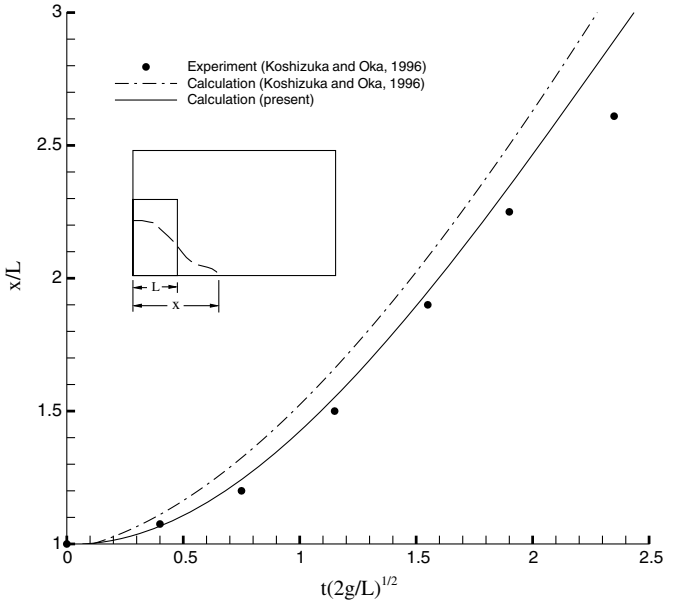

Fig. 3. Relationship between the nondimensional leading edge and the time after water column collapses

Water particles predicted by the numerical model at representative times are shown in Fig. 2. It is shown that the flow fields, including particle position and pressure distribution, are well predicted. During the water front evolution, before the downstream wall impact, the pressure field is almost consistent with shallow water wave condition, which is clearly seen in this figure. Fig. 3 indicates the comparison of the time variation for the position of the leading edge with experiments and computations from Koshizuka and Oka (1996). The relations between the normalized time $t(2g/L)^{1/2}$ (L is the initial width of the water column) and position of the leading edge $X = x/L$ are in good agreement. From the final part of the curves in this figure, the estimate of the typical velocity

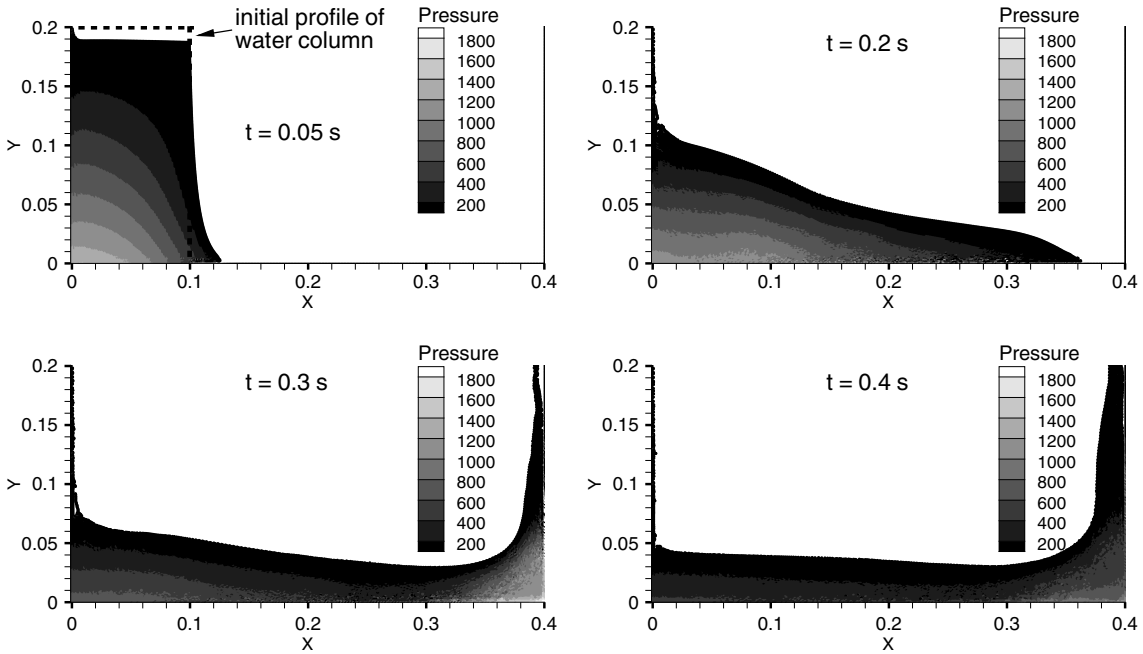

Fig. 2. Pressure distribution for the water dam break problem

J. Hydraul. Eng., 2016, 142(10): 04016032

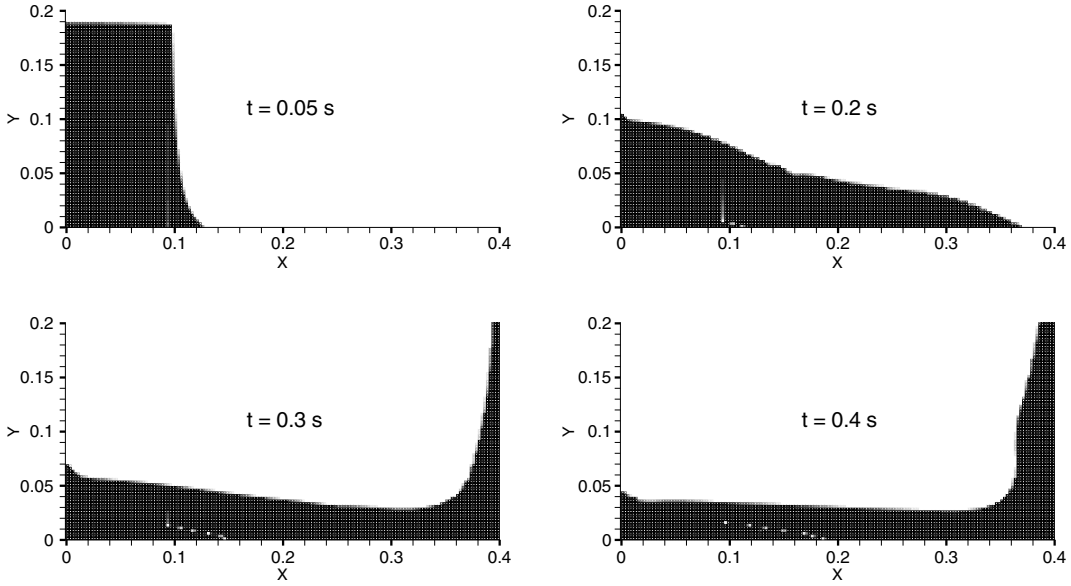

Fig. 4. Numerical simulation of water dam break problem using VOF method

V of the water front is approximately $dx/dt = 1.2\sqrt{2gL} \approx 1.69$ m/s. Considering the acceleration of water particles when impact onto the downstream wall, the choice for the typical velocity V of water particles to be 2.5 m/s is reasonable.

To quantify the error made with the SPH model, a convergence study is performed where the results obtained with the finite volume method (FVM) is taken as a reference. FVM is a mesh-based Eulerian method with the capability of capturing water free surface using the volume of fluid (VOF) technique (Hirt and Nichols 1981). Numerical simulation of the water dam break problem using VOF technique is shown in Fig. 4. The L_2 error is calculated based on the values of the horizontal velocity field u obtained by the SPH method and by FVM at all particles positions, through (Leroy et al. 2014)

$$L_2 = \sqrt{\frac{1}{V_T}\sum_a V_a \left(\frac{u_a^{\text{sph}} - u_a^{\text{ref}}}{u_{\max}}\right)^2} \tag{78}$$

where $V_T = \sum_a V_a$ = total volume of all the fluid particles; u^{sph} = velocity at time $t = 0.2$ s obtained by the SPH method; u^{ref} = velocity at the same instant obtained with VOF; and $u_{\max} = 2.5$ m/s is the typical velocity of the flow. Four particle resolutions, with the initial particle spacing h being equal to 0.01 m, 0.005 m, 0.0025 m, and 0.00125 m, respectively, are investigated. The results of the convergence study are shown in Fig. 5, where it appears that the order of convergence of the weakly compressible SPH (WCSPH) method is less than one, which is consistent with Leroy et al. (2014).

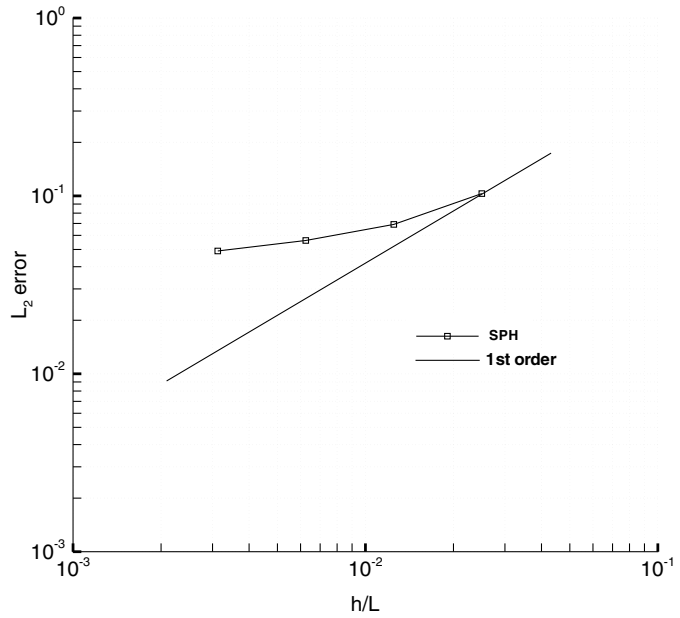

Fig. 5. Convergence study for the case of water dam break problem

Sand Column Collapse

Now the numerical model is validated for soil by applying it to another problem, namely the sand column collapse. This problem has been previously studied by many researchers (e.g., Bui et al. 2008; Chen and Qiu 2012; López et al. 2012). In this simulation, a sand column 0.2 m wide and 0.1 m high collapses at $t = 0$. Material constants for soil are listed in Table 2. In the simulation, a total of 12,800 soil particles are used, with an initial particle spacing of 0.00125 m. The time step size is set to $\Delta t = 5 \times 10^{-6}$ s.

Particle positions predicted by this numerical model at representative times is shown in Fig. 6. In this figure, the accumulated plastic shear strain indicated by color is computed by

Table 2. Parameters Used in the Computation for the Case of Sand Column Collapse

Property	Symbol	Value
Density of soil	$\tilde{\rho}_s$	2,650 kg/m^3
Young's modulus of soil	E	0.84 MPa
Bulk modulus	K	0.7 MPa
Poisson's ration of soil	ν	0.3
Internal friction angle of soil	θ	19.8°
Cohesion of soil	k_c	0
Sound speed in soil	c_s	20 m/s
Time step size	Δt	5×10^{-6} s

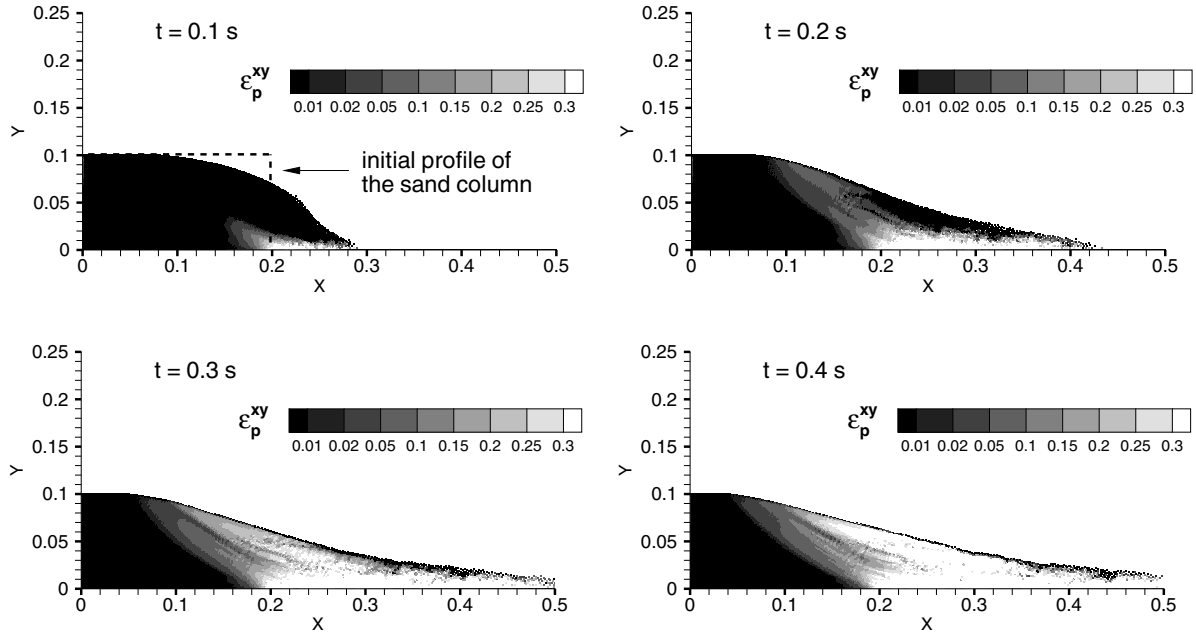

Fig. 6. Accumulated plastic shear strain ε_p^{xy} for sand column collapse

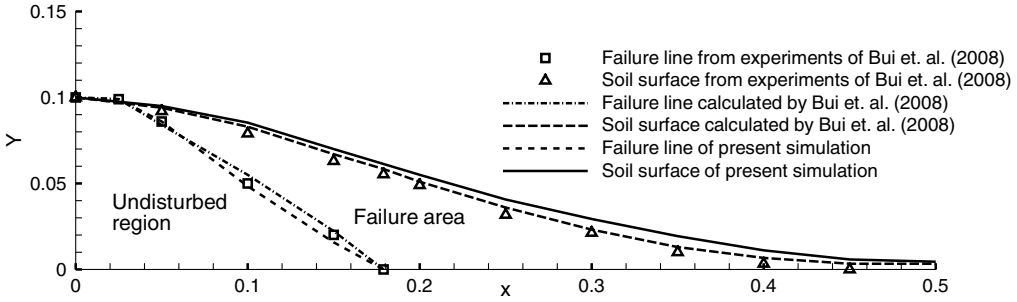

Fig. 7. Final soil surface and failure line

$$\epsilon_p^{xy} = \int_0^t \dot{\epsilon}_p^{xy} dt = \int_0^t \dot{\lambda} \frac{\partial H}{\partial \sigma^{xy}} dt = \int_0^t \dot{\lambda} \frac{\tau^{xy}}{2\sqrt{J_2}} dt \qquad (79)$$

where the time integration is also performed at half time steps as in Eq. (71). It is shown that plastic deformation mainly happen at the side slope region. An undisturbed region is observed after the collapse, which is consistent with the experimental observations of Lube et al. (2004, 2005). Fig. 7 compares the numerical results of final soil surface and failure line with experimental and computational results obtained by Bui et al. (2008). It indicates that the SPH model developed is capable of simulating the process of sand column collapse with satisfactory accuracy.

Flow through Porous Media

The drag force model is validated between different phases using the problem of flow in porous medium. As shown in Fig. 8, water flows in a U-tube from left to right through the soil sample under gravity. The geometry of the U-tube and the initial water level difference are shown in the figure. This problem has been previously studied by many researchers, e.g., Huang et al. (2013), with different geometries. In this test, the material parameters are: porosity

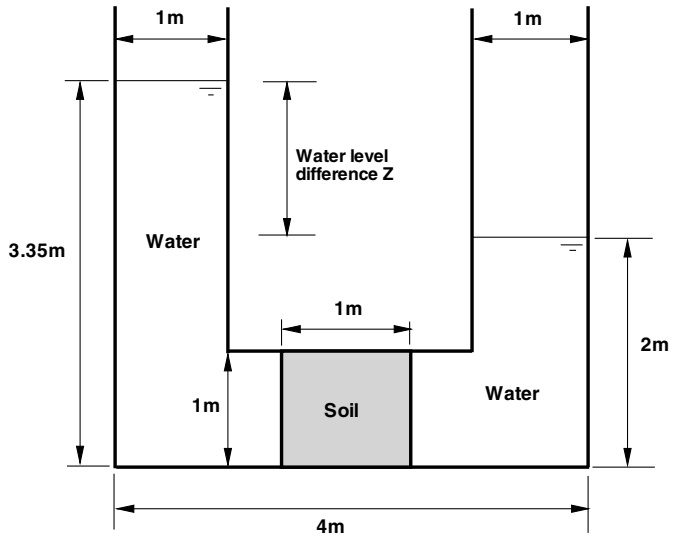

Fig. 8. Flow through porous media

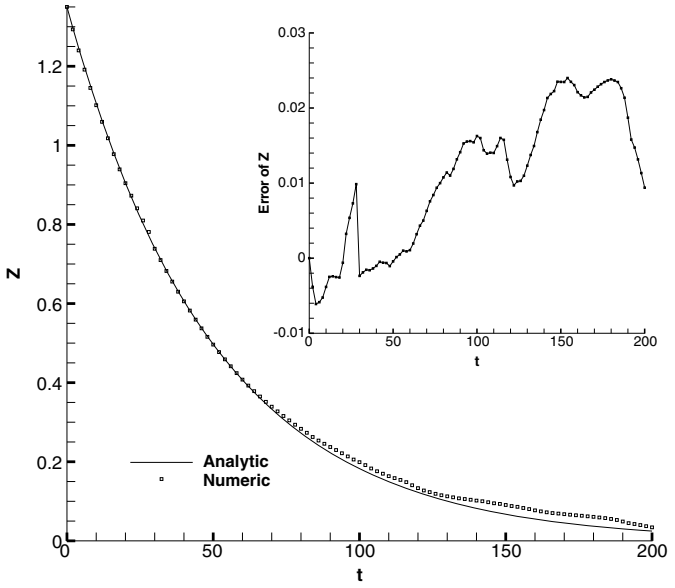

Fig. 9. Difference in water level for the U-tube flow problem

0.45; hydraulic conductivity 0.01 m/s; density of water 1,000 m^3/s; and density of soil 2,650 m^3/s. Numerical settings are: particle resolution 0.05 m; number of boundary particles 1,158; number of fluid particles 3,108; number of soil particles 567; and simulation duration 200s.

According to Darcy's law, the water level difference δZ at time t can be calculated by

$$\delta Z = \frac{\delta Z_0}{e^{\frac{2\,k(t-t_0)}{L}}} \tag{80}$$

where t_0 = initial time; δZ_0 = initial water level difference; k = hydraulic conductivity; and L = length of the soil sample. Darcy velocity in the soil can be calculated by $(1/2)(d\delta Z/dt)$. The theoretically calculated water level differences are shown in Fig. 9, along with the water level differences from the SPH simulation. Fig. 10 compares the horizontal Darcy velocity in the soil. The

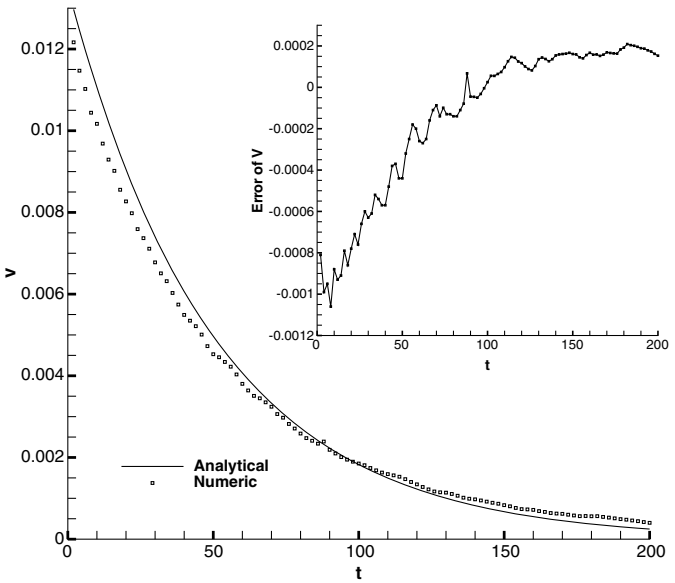

Fig. 10. Darcy velocity in the soil for the U-tube flow problem

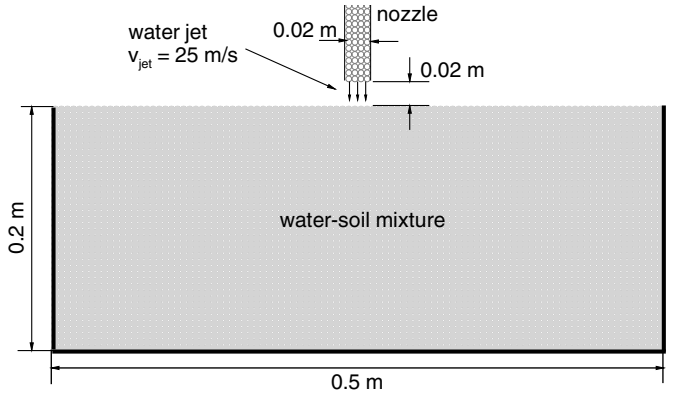

Fig. 11. Sketch of soil excavation by water jet

numerical errors compared with the analytical results are also shown in these figures. It is shown that numerical results agree well with the theoretical solutions.

Saturated Soil Excavation by Water Jets

Now the proposed SPH mixture model is applied to the problem of saturated soil excavation by high-velocity water jets. This problem has been studied by Bui et al. (2007) and more recently by Guo et al. (2013). However, in this section this problem is revisited using the mixture theory in order to reveal the effects of volume fraction on the mixture dynamics.

As seen in Fig. 11, the rectangular tank containing the soil stratum is 0.5 m in width and 0.2 m in height. The nozzle is in the middle above the tank with an impinging height of 0.02 m from the soil surface. The width of the nozzle is 0.02 m. The jetting velocity is 25 m/s. Material properties for soil and water are listed in Table 3. The sound speed c_s in soil is set to 215 m/s according to $c_s \approx \sqrt{K/\tilde{\rho}_s}$, where K is the bulk modulus of soil. The virtual sound speed c_f in water is 250 m/s. The initial values for the volume fractions of water and soil are set to $\phi_{f0} = \phi_{s0} = 0.5$. Jetting from the nozzle is pure water with $\phi_{f0} = 1$.

The water and soil materials are discretized by 4,000 particles for each phase, of which 3,150 are real particles and 850 are virtual particles for implementing the rigid wall boundary condition. The initial particle spacing is 0.005 m. The water jet is generated using water particles with the same initial spacing. Time step size Δt is set to 5.0×10^{-6} s.

Table 3. Material Properties Used in the Computation for the Soil Excavation by Waterjet

Property	Symbol	Value
True density of soil	$\tilde{\rho}_s$	2,700 kg/m^3
Young's modulus of soil	E	150 MPa
Bulk modulus of soil	K	125 MPa
Poisson's ratio of soil	ν	0.3
Internal friction angle of soil	θ	25°
Cohesion of soil	k_c	0
Initial volume fraction of soil	ϕ_{s0}	0.5
Hydraulic conductivity of soil	k	0.0005 m/s
Sound speed of soil	c_s	215 m/s
Dynamic viscosity of the water	μ	1.0×10^{-3} Pa · s
Initial true density of the water	$\tilde{\rho}_{f0}$	1000 kg/m^3
Virtual sound speed of water	c_f	250 m/s
Initial volume fraction of water	ϕ_{f0}	0.5

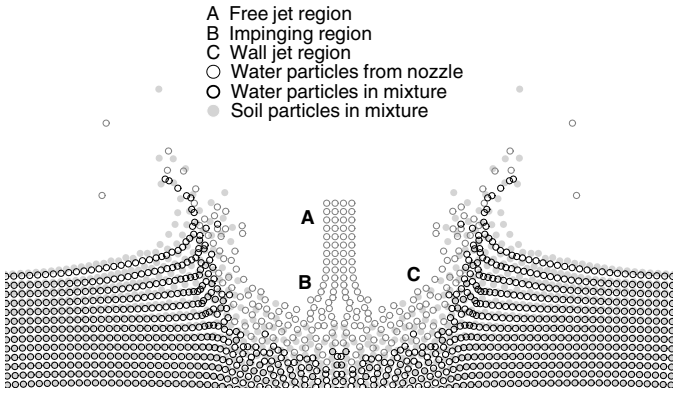

Fig. 12. Flow pattern of soil excavation by water jet

Fig. 12 shows the flow pattern during the water impinging process. Two interesting characteristics of the mixture flows are observed. First, the jet flow can be divided into three regions, i.e., the free jet region, the impingement region, and the wall jet region. In the free jet region, the jet essentially behaves as if there were no boundary. In the impingement region, the flow begins to stagnate and is redirected to flow along the soil surface. In the wall jet region, the flow behaves as a wall jet along the soil surface. The soil is eroded by the wall jet flow and soil particles are splashed together with the water particles. Second, during the excavation process, particles originally in the tank tend to flow over the tank. This can be explained by the reason that water is slightly compressible in SPH simulation. Because of the high pressure of the water jet, the water particles will force soil particles to move together, leading to the flow over of the water-soil mixture.

Fig. 13 compares numerical results obtained by the present SPH mixture model with that given by the SPH model of Bui et al. (2007). Soil surface at some representative times during the initial stage of the impingement are shown in this figure. It is shown that although numerical results obtained by both models are qualitatively consistent with each other, the SPH mixture model predicts a wider and shallower excavation hole. This is reasonable, bearing in mind that only part of the water pressure acts on the soil particles in the mixture model, as seen in Eq. (12). On the contrary, Bui's model, without considering the volume fractions, is in fact a two-fluid (i.e., pure water and pure soil) model with some interaction terms. Pure water contains more energy than water partially filled the same volume space with a fraction. Thus, a deeper and narrower excavation hole results in Bui's model.

Because of the high pressure in the impingement region, the water particles issued from the nozzle will merge into the soil particles in the tank. This will change the volume fractions of both water and soil near the excavation hole. With the proposed SPH mixture model, it is possible to investigate the temporal and spatial variations of the volume fraction. Fig. 14 shows the volume fraction

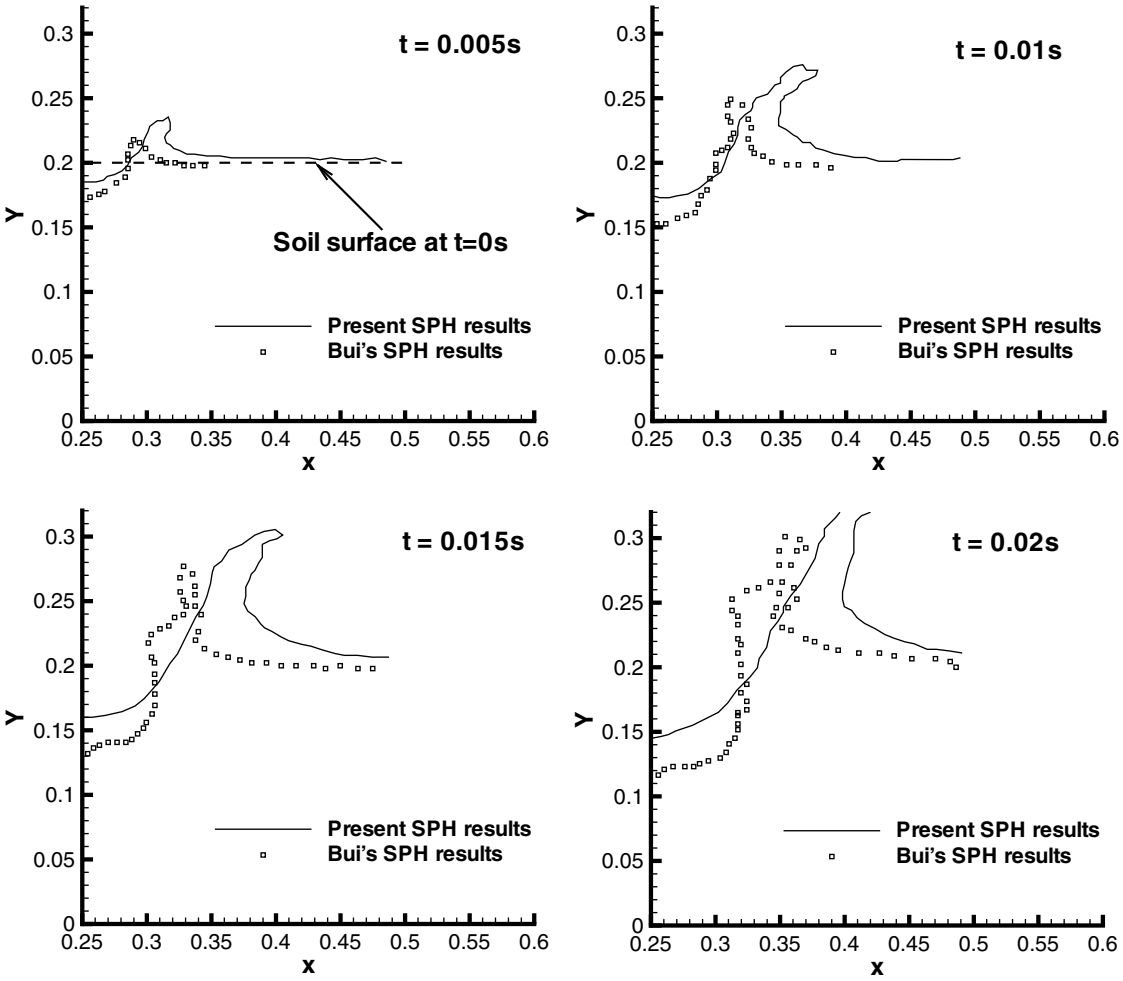

Fig. 13. Soil surface at representative times compared with that given by Bui et al. (2007) SPH model

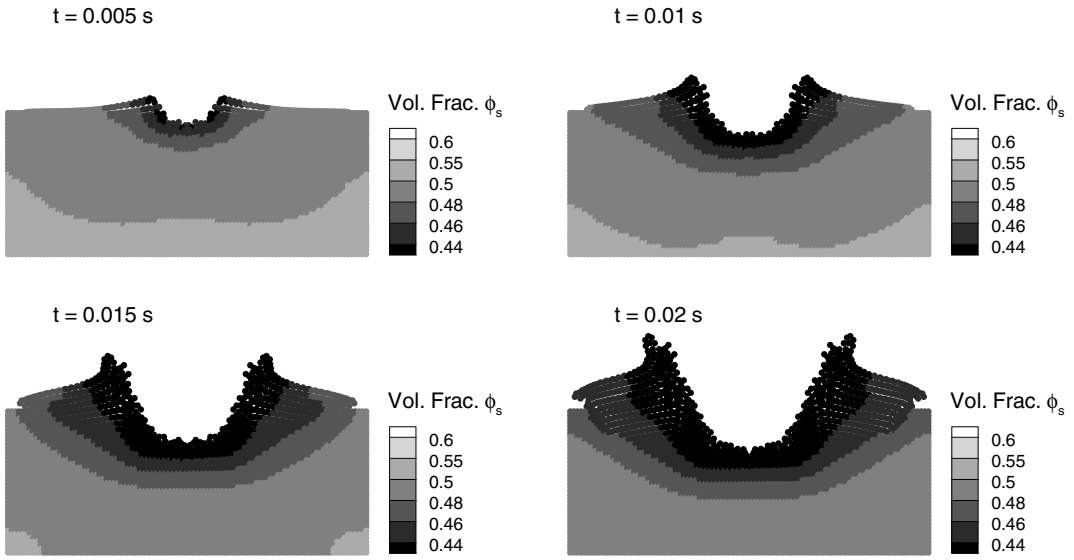

Fig. 14. Spatial and temporal variation of the volume fraction ϕ_s of soil

ϕ_s of soil at representative times. It is shown that ϕ_s decreases near the excavation hole. At the soil surface ϕ_s reaches its minimum due to the large water content there. Variation of ϕ_f is reversed.

For noncohesive saturated soil, the excavation hole is shallow and wide. Analysis of the soil failure mechanisms is helpful to understand the formation of the hole. Figs. 15 and 16 show the variations of soil pressure and accumulated plastic shear strain during the excavation process. It is shown that although the high pressure zone is at the impinging region, the plastic deformation is strongest at the wall jet region. At this region, soil undergoes severe erosion due to the strong reversed flow. This explains why a shallow and wide excavation hole forms in noncohesive saturated soil.

Hydraulic conductivity of soil has strong effects on the excavation. Generally speaking, lower hydraulic conductivity will lead to larger drag force. As a consequence, the soil particles and water particles adhere to each other and move together. Conversely, higher hydraulic conductivity will lead to lower drag force between the two phases. In this case, water particles can move through soil particles more easily, leading to stronger erosion of the soil. Fig. 17 shows excavations in soils with different hydraulic conductivities at $t = 0.01$ s. It is shown that soil particles with higher hydraulic conductivity are more easily eroded from the soil surface, leading to a larger excavation hole and stronger spray of particles.

As mentioned earlier, volume fractions play important roles in mixture dynamics, which can be investigated using the SPH model. Now the influence of initial water content on soil excavation is discussed. By varying the initial volume fractions of water or soil, water content in the mixture can be changed. Two different initial water contents are investigated, as seen in Fig. 18. It is shown that water content has great influence on the shape of the excavation hole. When the mixture contains more water, the excavation hole exhibits a "U" shape. It shows a "V" shape when the soil content is

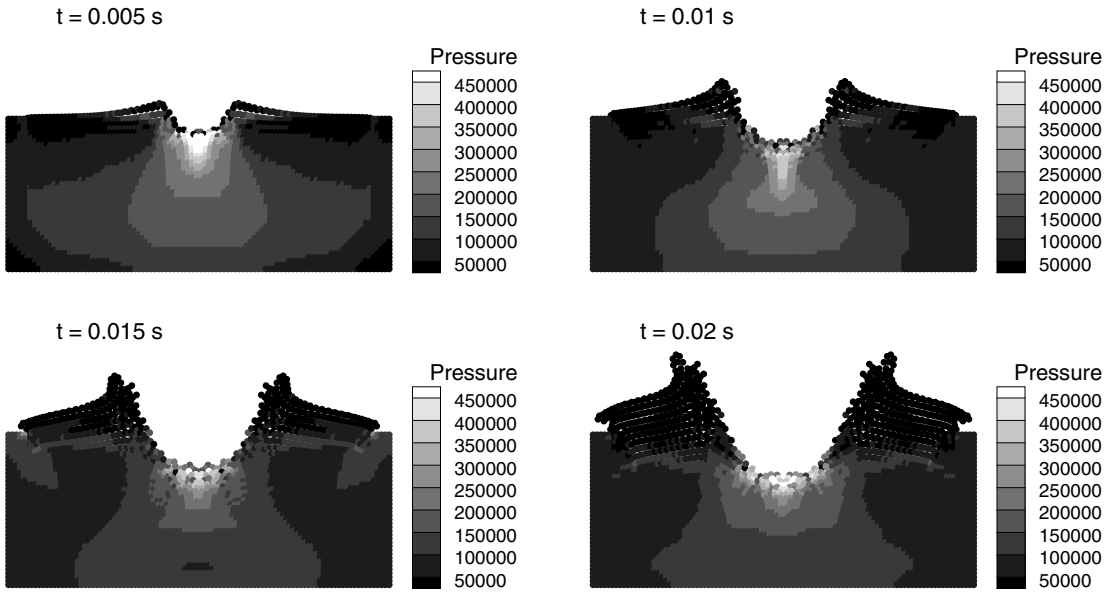

Fig. 15. Soil pressure distribution

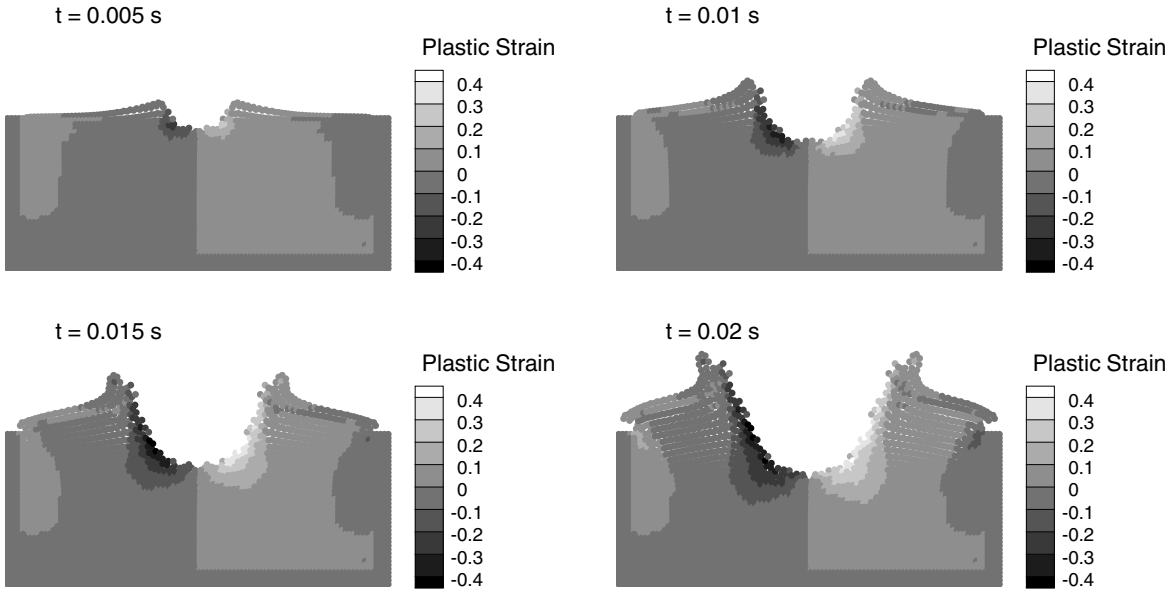

Fig. 16. Accumulated plastic shear strain ε_p^{xy} of soil

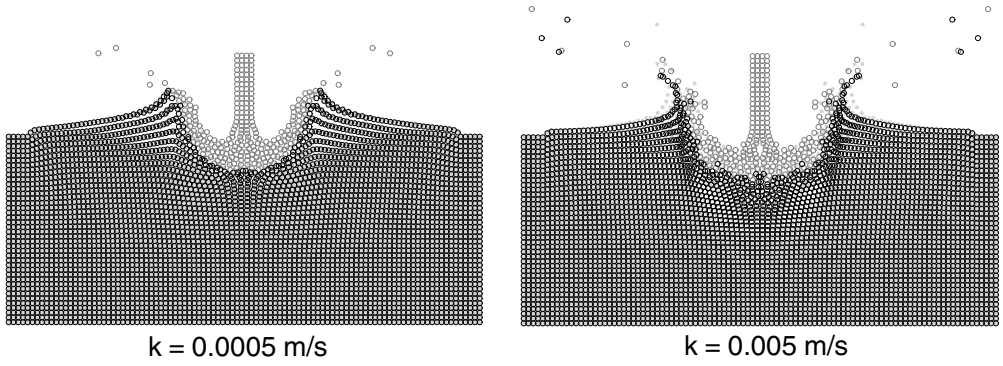

Fig. 17. Effects of hydraulic conductivity k on soil excavation at $t = 0.01$ s

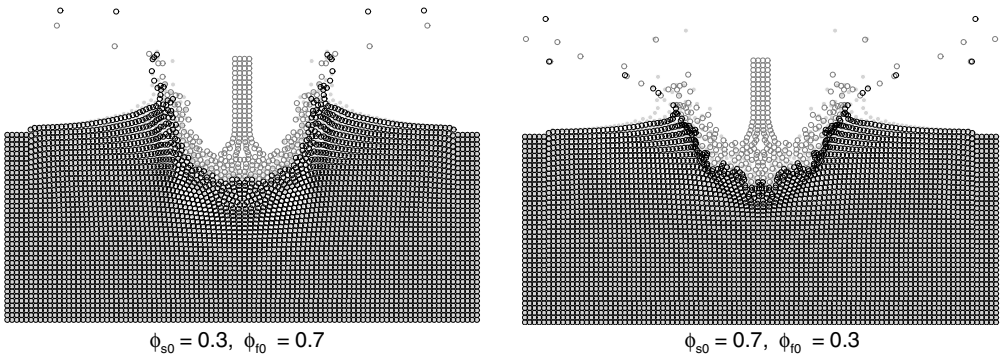

Fig. 18. Effects of initial volume fractions on soil excavation at $t = 0.01$ s

greater. This can be explained by the large resistance that water particles suffered in dense soil. Here the authors have shown again the advantages of the proposed SPH model in dealing with mixture flows. Many other water-soil interaction problems, such as underwater soil excavation or trenching, can also be explored using this method. However, these are topics of future research.

Conclusions

In this paper numerical simulation of water-soil interactions by means of SPH method is presented. In this study, the water-saturated soil is considered as a two-phase mixture. For each single phase (water and soil), conservation equations of mass

and momentum are formulated, taking the volume fraction into account. Interactions between water and soil are considered by the linear viscous drag force and the pore water pressure. The water is modeled by a Newtonian slightly-compressible fluid, while the soil is considered as an elastic-perfectly plastic material. A Drucker-Prager yield function with associated plastic flow rule is employed to describe the elastic-plastic behavior of the soil. The proposed model, including the model by Bui et al. (2008) as a particular case (i.e., dry soil), has the capability of dealing with saturated water-soil mixture flows.

Soil excavation by high-velocity water jet is investigated using the proposed approach. The same problem has been previously investigated by Bui et al. (2007) and Guo et al. (2013) but without taking the volume fractions into consideration. The present numerical simulation shows that initial volume fractions play an important role in the movements of saturated soil. With this two-phase SPH model it is possible to investigate the influence of the volume fractions on the mixture dynamics. In many situations, such as underwater jet trenching, excavation, or scour, it is necessary to consider the effects of volume fractions on the mixture dynamics. The proposed SPH approach provides an efficient tool to deal with such problems widely occurring in hydraulic engineering and geomechanics.

Future studies on the conservation properties and numerical accuracy of the proposed model, as well as the role of its parameters (e.g., artificial viscosity, hydraulic conductivity, etc.), could be considered. For the water dam breaking, a study on the time evolution of the system's total energy and its components (i.e., potential, kinetic, and internal) has been done by Colagrossi and Landrini (2003) to assess the model behavior. The study of the energy evolution for mixture flow is certainly useful when investigating conservation properties of the proposed model and therefore could be performed in the future.

The assumption of a constant hydraulic conductivity allows one to obtain reasonable results from an engineering point of view, as shown in this paper. However, theoretically speaking, the hydraulic conductivity should be influenced by the mechanical deformation of the soil, thus the improvement of numerical results by varying hydraulic conductivity could be tested in the future.

Acknowledgments

This numerical code has been developed based on the single-phase SPH code appended to the book by Liu and Liu (2003). The authors express their sincere thanks to the original developers. The authors are also grateful for the valuable discussions with Dr. H. H. Bui and Y. R. López on topics of computational plasticity. The authors also thank the anonymous reviewers for their critical comments, which are very helpful for improving the quality of this paper. This work is partly supported by National Key Basic Research Program of China (Approval No. 2014CB046801).

References

Aderibigbe, O. O., and Rajaratnam, N. (1996). "Erosion of loose beds by submerged circular impinging vertical turbulent jets." *J. Hydraul. Res.*, 34(1), 19–33.

Antuono, M., Colagrossi, A., Marrone, S., and Molteni, D. (2010). "Free-surface flows solved by means of SPH schemes with numerical diffusive terms." *Comput. Phys. Commun.*, 181(3), 532–549.

Bagnold, R. A. (1954). "Experiments on a gravity-free dispersion of large solid spheres in a Newtonian fluid under shear." *Proc. Roy. Soc. Lond. Ser. A Math. Phys. Sci.*, 225(1160), 49–63.

Bui, H. H., and Fukagawa, R. (2013). "An improved SPH method for saturated soils and its application to investigate the mechanisms of embankment failure: Case of hydrostatic pore-water pressure." *Int. J. Numer. Anal. Meth. Geomech.*, 37(1), 31–50.

Bui, H. H., Fukagawa, R., Sako, K., and Ohno, S. (2008). "Lagrangian meshfree particles method (SPH) for large deformation and failure flows of geomaterial using elastic-plastic soil constitutive model." *Int. J. Numer. Anal. Meth. Geomech.*, 32(12), 1537–1570.

Bui, H. H., Sako, K., and Fukagawa, R. (2007). "Numerical simulation of soil-water interaction using smoothed particle hydrodynamics (SPH) method." *J. Terramech.*, 44(5), 339–346.

Chen, W., and Qiu, T. (2012). "Numerical simulations for large deformation of granular materials using smoothed particle hydrodynamics method." *Int. J. Geomech.*, 10.1061/(ASCE)GM.1943-5622.0000149, 127–135.

Chen, W. F., and Mizuno, E. (1990). *Nonlinear analysis in soil mechanics: Theory and implementation*, Elsevier, Amsterdam, Netherlands.

Colagrossi, A., and Landrini, M. (2003). "Numerical simulation of interfacial flows by smoothed particle hydrodynamics." *J. Comput. Phys.*, 191(2), 448–475.

Crespo, A., Gómez-Gesteira, M., and Dalrymple, R. A. (2007). "Boundary conditions generated by dynamic particles in SPH methods." *CMC-Comput. Mater. Continua.*, 5(3), 173–184.

de Souza Neto, E. A., Peric, D., and Owen, D. R. J. (2011). *Computational methods for plasticity: Theory and applications*, Wiley, Chichester, U.K.

Drew, D. A. (1983). "Mathematical modeling of two-phase flow." *Annu. Rev. Fluid Mech.*, 15(1), 261–291.

Ferrand, M., Laurence, D. R., Rogers, B. D., Violeau, D., and Kassiotis, C. (2013). "Unified semi-analytical wall boundary conditions for inviscid, laminar or turbulent flows in the meshless SPH method." *Int. J. Numer. Meth. Fluids*, 71(4), 446–472.

Fourtakas, G., Rogers, B. D., and Laurence, D. R. (2013). "Modelling sediment resuspension in industrial tanks using SPH." *La Houille Blanche*, 2, 39–45.

Gingold, R. A., and Monaghan, J. J. (1977). "Smoothed particle hydrodynamics: Theory and application to non-spherical stars." *Mon. Not. R. Astron. Soc.*, 181(3), 375–389.

Gomez-Gesteira, M., Rogers, B., Crespo, A., Dalrymple, R., Narayanaswamy, M., and Dominguez, J. (2012). "SPHysics—Development of a free-surface fluid solver—Part 1: Theory and formulations." *Comput. Geosci.*, 48, 289–299.

Gray, J., Monaghan, J., and Swift, R. (2001). "SPH elastic dynamics." *Comput. Meth. Appl. Mech. Eng.*, 190(49–50), 6641–6662.

Guo, Z. M., Shao, J. R., Shen, Y. X., and Liu, M. B. (2013). "Numerical simulation of soil-water jet interaction with smoothed particle hydrodynamics." *3rd Int. Conf. on Particle-Based Methods—Fundamentals and Applications, PARTICLE 2013*, M. Bischoff, E. Oñate, D. R. J. Owen, E. Ramm, and P. Wriggers, eds., Stuttgart, Germany, 418–427.

Hirt, C. W., and Nichols, B. D. (1981). "Volume of fluid (vof) method for the dynamics of free boundaries." *J. Comput. Phys.*, 39(1), 201–225.

Huang, Y., Zhang, W., Dai, Z., and Xu, Q. (2013). "Numerical simulation of flow processes in liquefied soils using a soil-water-coupled smoothed particle hydrodynamics method." *Nat. Hazard.*, 69(1), 809–827.

Idelsohn, S. R., Oñate, E., and Pin, F. D. (2004). "The particle finite element method: A powerful tool to solve incompressible flows with free-surfaces and breaking waves." *Int. J. Numer. Meth. Eng.*, 61(7), 964–989.

Iverson, R. M., and Denlinger, R. P. (2001). "Flow of variably fluidized granular masses across three-dimensional terrain: 1. Coulomb mixture theory." *J. Geophys. Res.*, 106(B1), 537–552.

Koshizuka, S., and Oka, Y. (1996). "Moving-particle semi-implicit method for fragmentation of incompressible fluid." *Nucl. Sci. Eng.*, 123(3), 421–434.

Leroy, A., Violeau, D., Ferrand, M., and Kassiotis, C. (2014). "Unified semi-analytical wall boundary conditions applied to 2-D incompressible SPH." *J. Comput. Phys.*, 261, 106–129.

Liu, G. R., and Liu, M. B. (2003). *Smoothed particle hydrodynamics: A meshfree particle method*, World Scientific, Singapore.

López, Y. R., Roose, D., and Morfa, C. R. (2012). "Dynamic refinement for SPH simulations of post-failure flow of non-cohesive soil." *Proc., 7th Int. SPHERIC workshop*, Prato, Italy.
Lube, G., Huppert, H. E., Sparks, R. S. J., and Freundt, A. (2005). "Collapses of two-dimensional granular columns." *Phys. Rev. E*, 72(4), 1301–1310.
Lube, G., Huppert, H. E., Sparks, R. S. J., and Hallworth, M. A. (2004). "Axisymmetric collapses of granular columns." *J. Fluid Mech.*, 508, 175–199.
Lucy, L. B. (1977). "A numerical approach to the testing of the fission hypothesis." *Astronom. J.*, 82(12), 1013–1024.
Manenti, S., and Sibilla, S., Gallati, M., Agate, G., and Guandalini, R. (2012). "SPH simulation of sediment flushing induced by a rapid water flow." *J. Hydraul. Eng.*, 10.1061/(ASCE)HY.1943-7900.0000516, 272–284.
Marrone, S., Antuono, M., Colagrossi, A., Colicchio, G., Touzé, D. L., and Graziani, G. (2011a). "F020δ-SPH model for simulating violent impact flows." *Comput. Meth. Appl. Mech. Eng.*, 200(13–16), 1526–1542.
Marrone, S., Colagrossi, A., Antuono, M., Lugni, C., and Tulin, M. (2011b). "A 2D+t SPH model to study the breaking wave pattern generated by fast ships." *J. Fluids Struct.*, 27(8), 1199–1215.
Mazurek, K. A., Rajaratnam, N., and Sego, D. C. (2001). "Scour of cohesive soil by submerged circular turbulent impinging jets." *J. Hydraul.*, 10.1061/(ASCE)0733-9429(2001)127:7(598), 598–606.
Monaco, A. D., Manenti, S., Gallati, M., Sibilla, S., Agate, G., and Guandalini, R. (2011). "SPH modeling of solid boundaries through a semi-analytic approach." *Eng. Appl. Comput. Fluid Mech.*, 5(1), 1–15.
Monaghan, J. J. (1994). "Simulating free surface flows with SPH." *J. Comput. Phys.*, 110(2), 399–406.
Monaghan, J. J. (1997). "Implicit SPH drag and dusty gas dynamics." *J. Comput. Phys.*, 138(2), 801–820.
Monaghan, J. J. (2000). "SPH without a tensile instability." *J. Comput. Phys.*, 159(2), 290–311.
Monaghan, J. J. (2005). "Smoothed particle hydrodynamics." *Rep. Progr. Phys.*, 68(8), 1703–1759.
Monaghan, J. J., and Kocharyan, A. (1995). "SPH simulation of multiphase flow." *Comput. Phys. Commun.*, 87(1–2), 225–235.
Nield, D. A., and Bejan, A. (2006). *Convection in porous media*, 3rd Ed., Springer, New York.
Perng, A. T. H., and Capart, H. (2008). "Underwater sand bed erosion and internal jump formation by travelling plane jets." *J. Fluid Mech.*, 595, 1–43.
Pitman, E. B., and Le, L. (2005). "A two-fluid model for avalanche and debris flows." *Phil. Trans. Roy. Soc. A Math., Phys. Eng. Sci.*, 363(1832), 1573–1601.
Pudasaini, S. P. (2012). "A general two-phase debris flow model." *J. Geophys. Res.*, 117(F3), F03010.
Savage, S. B., and Hutter, K. (1989). "The motion of a finite mass of granular material down a rough incline." *J. Fluid Mech.*, 199, 177–215.
Ulrich, C., Leonardi, M., and Rung, T. (2013). "Multi-physics SPH simulation of complex marine-engineering hydrodynamic problems." *Ocean Eng.*, 64, 109–121.
Violeau, D. (2012). *Fluid mechanics and the SPH method: Theory and applications*, Oxford University Press, Oxford, U.K.
Violeau, D., and Issa, R. (2007). "Numerical modelling of complex turbulent free-surface flows with the SPH method: An overview." *Int. J. Numer. Meth. Fluids*, 53(2), 277–304.
Wang, Y., and Hutter, K. (1999a). "A constitutive model of multiphase mixtures and its application in shearing flows of saturated solid-fluid mixtures." *Granular Matter*, 1(4), 163–181.
Wang, Y., and Hutter, K. (1999b). "A constitutive theory of fluid-saturated granular materials and its application in gravitational flows." *Rheologica Acta*, 38(3), 214–223.
Wendland, H. (1995). "Piecewise polynomial, positive definite and compactly supported radial functions of minimal degree." *Adv. Comput. Math.*, 4(1), 389–396.
Yeh, P. H., et al. (2009). "Large-scale laboratory experiment on erosion of sand beds by moving circular vertical jets." *Ocean Eng.*, 36(3–4), 248–255.